UST CORRECTIVE ACTION TECHNOLOGIES:
Engineering Design of
Free Product Recovery Systems

by

Jack C. Parker,
Dan W. Waddill,
and
Jeffrey A. Johnson
Environmental Systems & Technologies, Inc.
Blacksburg, Virginia 24060

Project Officer

Chi-Yuan Fan
Land Remediation & Pollution Control Division
National Risk Management Research Laboratory
Edison, New Jersey 08837

Disclaimer

The information in this document has been partially funded by the U.S. Environmental Protection Agency (EPA) under Contract No. 68-C2-0108 to International Technology Corporation and its subcontractor Environmental Systems and Technologies, Inc. It has been subjected to the Agency's peer and administrative review, and has been approved for publication. Mention of trade names or commercial products does not constitute endorsement or recommendation for use.

Foreword

The U.S. Environmental Protection Agency is charged by Congress with protecting the Nation's land, air, and water resources. Under a mandate of national environmental laws, the Agency strives to formulate and implement actions leading to a compatible balance between human activities and the ability of natural systems to support and nurture life. To meet this mandate, EPA's research program is providing data and technical support for solving environmental problems today and building a science knowledge base necessary to manage our ecological resources wisely, understand how pollutants affect our health, and prevent or reduce environmental risks in the future.

The National Risk Management Research Laboratory is the Agency's center for investigation of technological and management approaches for reducing risks from threats to human health and the environment. The focus of the Laboratory's research program is on methods for the prevention and control of pollution to air, land, water, and subsurface resources; protection of water quality in public water systems; remediation of contaminated sites and ground water; and prevention and control of indoor air pollution. The goal of this research effort is to catalyze development and implementation of innovative, cost-effective environmental technologies; develop scientific and engineering information needed by EPA to support regulatory and policy decisions; and provide technical support and information transfer to ensure effective implementation of environmental regulations and strategies.

This publication has been produced as part of the Laboratory's strategic long-term research plan. It is published and made available by EPA's Office of Research and Development to assist the user community and to link researchers with their clients.

E. Timothy Oppelt, Director
National Risk Management Research Laboratory

Abstract

The objective of this project was to develop a technical assistance document for assessment of subsurface hydrocarbon spills and for evaluating effects of well placement and pumping rates on separate phase plume control and on free product recovery. Procedures developed for estimation of hydrocarbon spill volume include interpolation and spatial integration of measurements from soil cores, and fluid level data from monitoring wells. The first method involves vertical integration of soil concentration measurements to yield oil volume or species mass per unit area followed by kriging and areal integration to estimate the total mass or volume within the measurement zone. This method is especially well suited to determine the amount of residual product in the unsaturated zone. The second method involves kriging of well fluid levels, calculation of free oil volume per area using a physically based model for vertically hydrostatic three phase fluid distributions that converts well product thickness to soil product thickness, followed by areal integration to estimate the volume of free product floating on the water table. A procedure is presented to evaluate effects of steady-state water pumping from multiple point sources on the oil flow gradients to evaluate if hydraulic control of plume spreading will be obtained for a selected system of pumping wells and/or trenches. Estimates of residual oil in the unsaturated and saturated zones are made from three phase capillary pressure-saturation relations and from the initial oil thickness distributions and computed water table drawdown, which enable determination of the recoverable spill volume for alternative well configurations. A variety of practical examples and case studies are presented to illustrate the methodology and to demonstrate how various factors interact to affect free product recovery system effectiveness. The applicability of trenches and vacuum enhanced product recovery to hydrocarbon spills is also discussed.

iv

Contents

Tables

Figures

Figures (continued)

Acknowledgment

Section 1

Introduction

The characterization and remediation of groundwater contamination is one of the most challenging problems facing the environmental field today. In particular, the problems caused by hydrocarbon spillage and disposal are both widespread and complex. For example, it has been estimated that over 75,000 underground storage tanks annually release 11 million gallons of gasoline to the subsurface (*Hall and Johnson,* 1992). Given that from 100 to 150 compounds can be identified in a typical gasoline, each having distinct physical and chemical characteristics, significant scientific and technical knowledge is required to successfully manage the potential environmental impacts and health risks associated with hydrocarbon releases in the subsurface.

Hydrocarbons are fluids that are immiscible with water and as such are considered nonaqueous phase liquids (NAPLs). In general, most hydrocarbon compounds are less dense than water and are termed light nonaqueous phase liquids (LNAPLs). When released in the subsurface, LNAPLs remain distinct fluids and flow separately from the water phase. The downward migration in the vadose zone is generally rapid, and depending upon the complexity of the heterogeneities in the soil, may form an intricate network of pathways. Once in the vicinity of the capillary fringe, hydrocarbons will spread horizontally with minimal penetration below the water table due to buoyancy. Contact with groundwater as well as infiltrating recharge causes chemical constituents to dissolve from the hydrocarbon into the groundwater resulting in contamination of the aquifer. Further, volatile constituents may partition into and move in the soil vapor. Through this complex array of physical and chemical processes, the hydrocarbon continually changes. It is due to these processes that the characterization, containment, and remediation of hydrocarbons pose unique and difficult problems for the environmental professional.

The first step in assessing a hydrocarbon spill generally involves delineating the vertical and horizontal extent of soil and groundwater contamination. Characterization may include visual observations of soil borings, in situ vapor readings, laboratory analysis of soil concentrations, measurements of fluid levels and dissolved and vapor concentrations in monitoring wells or probes, and surface or subsurface geophysical methods.

Measurements of soil concentrations (e.g., total petroleum hydrocarbons or individual species) provide the most reliable quantitative information on the actual volume or mass of hydrocarbon in the subsurface. However, since laboratory analyses of soil samples are costly and are not practically amenable in monitoring temporal changes (that occur over time), the estimation of spill volume from fluid level measurements in monitoring wells has a much greater

1

practical value. Unfortunately, estimation of hydrocarbon volume from well fluid level data is less straightforward than estimation from soil concentration data. A general lack of understanding in this area, compounded by promulgation of methods of dubious validity and poor accuracy, have resulted in widespread misunderstanding.

It is well known that the hydrocarbon volume in the soil per unit area ("oil specific volume") is significantly less than well product thickness (a.k.a."apparent product thickness") (e.g., *van Dam*, 1967). Using a very simplified theoretical approach, *de Pastrovich et al.* (1979) suggested that well product thickness will typically be about four times greater than the soil zone thickness within which free product occurs (a.k.a., "soil product thickness"). *Hall et al.* (1984) investigated the relationship between soil product thickness and well product thickness in the laboratory and proposed an empirical relation to correct for discrepancies in the method of de Pastrovich. Laboratory investigations by *Hampton and Miller* (1988) found the methods of both de Pastrovich and Hall lacked accuracy, and they questioned the relevance of estimating soil product thickness, since it does not directly relate to oil specific volume, which is of more fundamental interest.

A theoretically based method for estimating oil specific volume from well product thickness was developed and reported independently by *Lenhard and Parker* (1990) and *Farr et al.* (1990). The method is based on the assumption of vertical equilibrium pressure distributions near the water table, which can be inferred from well fluid levels. From the fluid pressure distributions and a general model for three phase capillary pressure relations, vertical oil saturation distributions are computed and integrated to yield oil specific volume.

In addition to "free" product that is sufficiently mobile to enter a monitoring (or recovery) well, a significant portion of the total spill volume may occur as "residual product," confined as hydraulically isolated blobs or thin films of oil that are effectively prevented from moving by capillary forces. Changes in water table elevation will generally result in increased residual volumes over time. These fluctuations may result from natural recharge variations, drawdown or injection as well as air-oil and oil-water fluid interface elevation changes due to plume spreading or recovery operations. The key to maximizing product recovery from spill sites involves minimizing the volume of residual product that is induced as a result of recovery system operations.

Product recovery systems are often implemented based solely on containment considerations. That is, trenches and/or wells are located to prevent further plume migration. While such an approach may be effective in a limited sense, it disregards an evaluation of efficiency, as plume containment can be achieved using many different well/trench configurations and operating conditions. Depending on the regulatory requirements, risk characteristics, and hence the cleanup objectives, "efficiency" may have different meanings: total volume of product recovered, ratio of product recovered per gallon of water pumped, time to reach asymptotic recovery, capital and operating costs, etc. Once specific objectives have been defined, various design strategies may be evaluated to obtain the desired "efficiency."

Recent advances in numerical models for multiphase flow (*ES&T*, 1994 abc; *Parker et al.*, 1990, 1991) along with increases in microcomputer speed and capability have made it possible to perform sophisticated analyses to assess the effects of various design options and natural events on spill migration and recovery system performance. Although such analyses require significant computational effort and personnel commitment, which can limit their applicability to large or high-risk sites, their use is essential to fully evaluate the potential complexities of hydrocarbon assessment and remediation.

The purpose of this report is to outline a set of accurate yet computationally simple protocols for spill site assessment and remedial design for hydrocarbon spills. The protocols provide a practical means to improve the quality and to reduce the costs of site investigations and remedial actions at hydrocarbon spill sites. The methods are particularly suited to small spills, for which more sophisticated analyses may not be warranted, and as a preliminary modeling tool for larger sites.

This report discusses the physical processes that control hydrocarbon retention, movement and recovery. It describes algorithms for estimating free and residual hydrocarbon volumes from monitoring well and soil boring data, as well as for evaluating plume migration and containment, and product recovery volume and time as affected by well and/or trench placement and operation. The methodologies are simple, and although somewhat laborious for hand calculations, require minimal computational effort for readily available desktop computers. The algorithms in this report have been implemented in the program SpillCAD (*ES&T*, 1994c).

Section 2

Basics of Hydrocarbon Behavior

2.1 Water, Air, and NAPL Flow

A good place to start to develop an understanding of how hydrocarbons move in the subsurface is Darcy's law. This well known relationship, which is the cornerstone of groundwater hydrology, may be generalized to describe the movement of nonaqueous phase liquids (NAPLs) and air in soil. The general form of Darcy's law may be written as

$$q_p = -\frac{k_{rp}K_{sw}}{\eta_{rp}}\left(\frac{\delta h_p}{\delta x} + \rho_{rp}u\right)$$
(2.1)

where q_p is the Darcy velocity of fluid p (e.g., p = air, NAPL or water), x is distance, h_p is the water height equivalent pressure of phase p, K_{sw} is the saturated hydraulic conductivity of the soil to water, k_{rp} is the p-phase relative permeability, η_{rp} is the ratio of p-phase to water viscosity, ρ_{rp} is the p-phase specific gravity, and u is a gravitational vector that is one in the vertical direction and zero in the horizontal direction.

Darcy's law says that fluid flows in response to a pressure gradient and to gravity at a rate inversely proportional to the fluid viscosity, and directly proportional to the *relative permeability*. Relative permeability is a factor that reflects the ability of fluid to move through the pore space when it is partially occupied by other fluids. When p-phase fluid completely fills the pore space, the relative permeability for the phase is one, and when no mobile p-phase is present the relative permeability is zero.

Relative permeability depends on the fraction of the pore space filled with p-phase (i.e., p-phase "saturation"), but more importantly on the hydraulic radius of the flow channels created by the pore geometry and by the interfaces with other fluids. Thus, narrow flow channels exhibit a smaller relative permeability than wide channels, even if the saturation is the same.

4

Understanding how multiple fluids interact within a porous medium and compete for the available pore space is the key to understanding relative permeability and, more fundamentally, to the relationship between phase pressures and phase saturations. This will be considered in the next section.
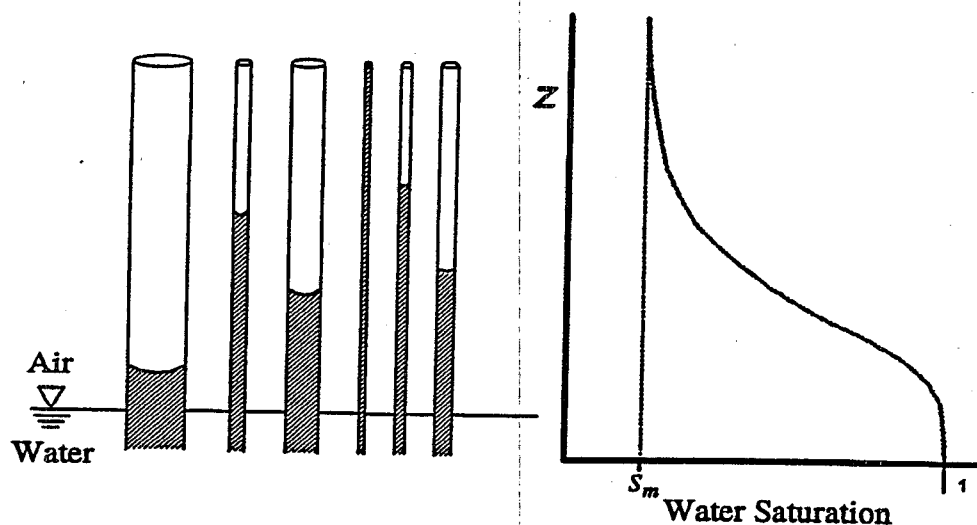
Figure 2-1. Water retention in a collection of capillary tubes.

2.2   Capillary Retention Relations

Two Phase Capillary Pressure Relations
In the absence of NAPL, water and air may coexist in the pore space and the saturation of each phase will depend on the pressure difference between the fluid phases, which is referred to as the *capillary pressure*. When two immiscible fluids are in contact, the pressure difference between the phases will induce a curvature to the interface. Since pore geometry ultimately controls interface curvature in a porous medium, as the capillary pressure changes, the interfaces recede or expand into different pores and the fluid saturations change. This may be more clearly understood by consideration of an idealized representation of a porous medium consisting of a bundle of parallel capillary tubes (Figure 2-1). If the bundle is placed in contact with a free water surface (i.e., plane of zero capillary pressure, a.k.a. the "water table"), and allowed to equilibrate, water will rise in the tubes to a height at which capillary

forces are balanced by gravitational forces. The Laplace capillary equation relates interface curvature to capillary pressure as

$$h_c = \frac{2\sigma}{R}$$
(2.2)

where h_c is the capillary pressure head (the difference between air and water pressure heads), σ is the interfacial tension between the fluids (here, air and water), and R is the radius of curvature of the air-water interface. At equilibrium, h_c corresponds to the height of capillary rise above the free water surface, and if the solid surface is readily wettable by water, the radius of curvature corresponds to the tube radius . As we view the system from bottom to top, we notice that as the capillary pressure increases, the fraction of the pore space occupied by water (i.e., water saturation) decreases (Figure 2-1).

This provides a simple illustration of the concept of a "capillary fringe" above a water table. It should be emphasized that the transition from a water-saturated condition is gradual, due to the distribution of pores of different sizes. The example also demonstrates the relationship between capillary pressure and phase saturation and its relationship with the pore size distribution of the porous medium.

Of course, pores in real soils are not really straight tubes, but rather channels of complex shapes that exhibit cross sections of varying size and shape along their length. The capillary pressure required to remove water from a pore of variable cross section diameter will be controlled by the smallest pore throat, while drainage will be controlled by the largest pore diameter (Figure 2-2). This results in the dependence of water saturation in the pore space on the history of capillary pressure changes -- a phenomenon referred to as *hysteresis*. As a result, lower water saturations occur at a given capillary pressure when capillary pressure is decreasing ("imbibition) than when capillary pressure is increasing ("drainage"). Within the limits of the primary imbibition and drainage curves, scanning curves define wetting and drying paths for less extreme water content changes (Figure 2-3). Futhermore, during imbibition displacement of the nonwetting phase (e.g., air or NAPL) is incomplete due to pore bypassing by the wetting phase, resulting in residual nonwetting phase in the soil. The maximum residual nonwetting phase will occur for the primary imbibition path (Figure 2-3).
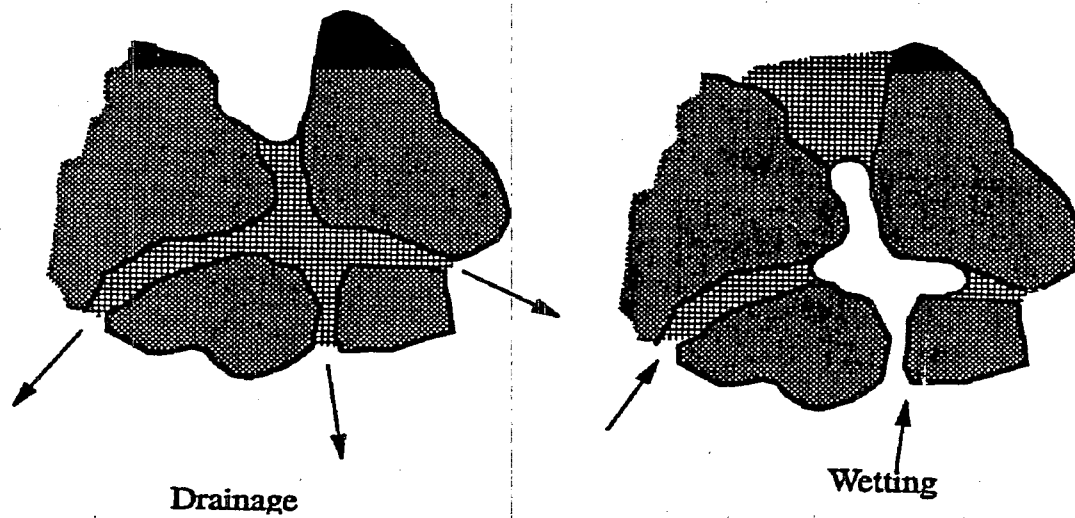
Figure 2-2. Water distribution in pores during imbibition and drainage.
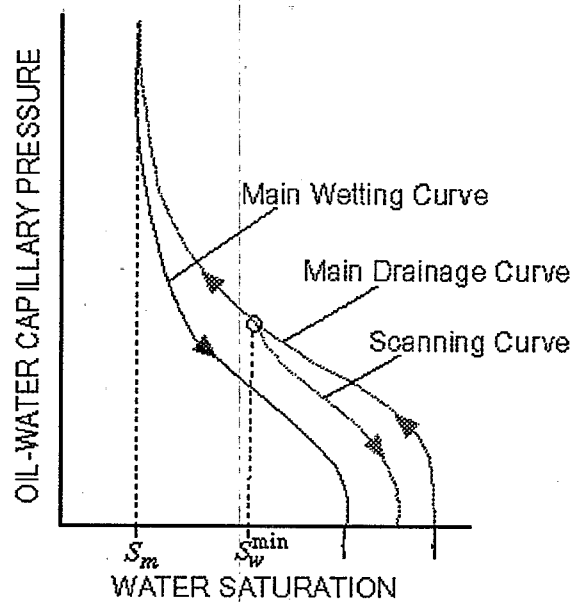
Figure 2-3. Hysteresis in capillary pressure function during drainage and imbibition.

7

The shape of the curve relating water saturation to air-water capillary pressure can be described parametrically using an empirical formula developed by *van Genuchten* (1980) given by

$$S_w = (1 - S_m)(1 + (\alpha h_{aw})^n)^{-m} + S_m$$

(2.3)

where S_w is the water saturation corresponding to a given air-water capillary pressure h_{aw}, S_m is an apparent "irreducible" water saturation, α and n are van Genuchten parameters for the soil, and $m = 1 - 1/n$. *Kool and Parker* (1988) have shown that for a wide range of soils, α for imbibition is approximately two times the value of α for drainage.

Because soil grain size distribution, in conjunction with grain packing geometry, controls the soil pore size distribution, soils of different types will exhibit different saturation-capillary pressure relations. Typical capillary pressure functions for two soil types are shown in Figure 2-4. Finer materials require larger capillary pressures before air can occupy a significant fraction of the pore space. Finer materials also tend to hold more water at very high capillary pressures, when the water content tends to approach an apparently "irreducible" value by water held tightly due to short range attractive forces between water molecules and solid surfaces.
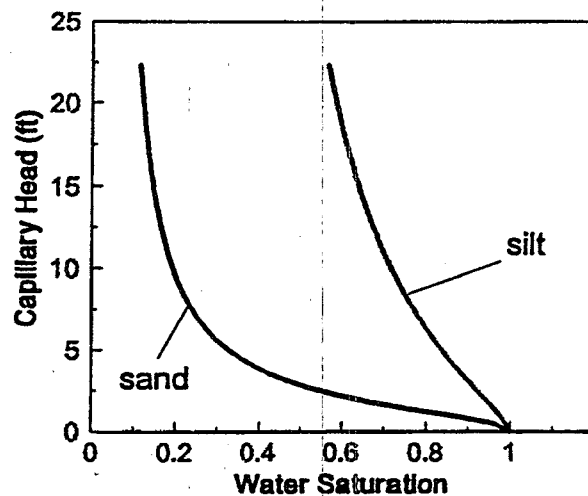
Figure 2-4. Drainage air-water capillary pressure functions for different soils

When a third fluid enters the picture (i.e., NAPL or "oil" for brevity), the distribution of fluids in the pore space gets more complicated, but the same physical processes still control the system. The first important issue to understand is the relative "wettability" of the different fluids in the porous media. The fluid of highest wettability by definition has the greatest affinity for the solid grains that make up the porous medium, while the fluid of lowest wettability will occupy pores farthest from the solid phase. Most geologic media are "water-wet," meaning that water is the phase of highest wettability. Air is usually the phase of lowest wettability, and NAPLs exhibit intermediate wettability. Under such circumstances, the distribution of fluids in the pore space will appear something like that shown in the illustration of Figure 2-5.

When three fluids (air, oil and water) jointly occupy the pore space, fluid-fluid interfaces will occur on the pore scale between the fluids of highest and intermediate wettability (i.e., water and oil) and between the fluids of intermediate and low wettability (i.e., oil and air). Capillary pressures may be defined for each of these interface pairs. The radius of curvature of oil-water interfaces will be controlled by the oil-water capillary pressure (pressure difference between oil and water), and air-oil interface curvatures will be controlled by the air-oil capillary pressure (difference between air and oil pressure). The Laplace capillary equation (eq. 2.2) applies to both interfaces, if the appropriate capillary pressure and interfacial tension are used.
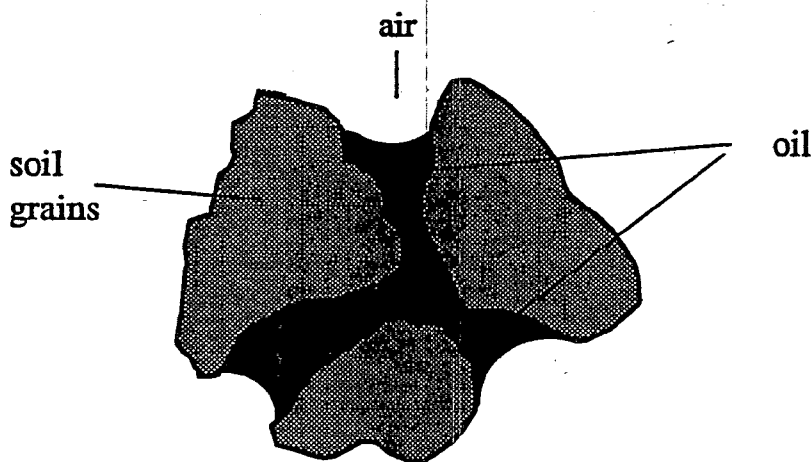
Figure 2-5. Distribution of air, oil and water in a porous medium.

If wettability follows the usual order, the radius of curvature of the oil-water interfaces will be controlled by the fraction of pore space occupied by water, while the radius of curvature of air-oil interfaces will depend on the fraction of pores filled with oil and water, since both phases are less wettable than air. Therefore, water saturation is expected to be a function of oil-water capillary pressure, and total liquid saturation is expected to be a function of air-oil capillary pressure. If the pore size distribution is time invariant, the Laplace capillary equation indicates that capillary pressure function for two and three fluid phase systems should be related by

$$S_w^{II}(h_{aw}) = S_w^{III}(\beta_{ow} h_{ow}) = S_t^{III}(\beta_{ao} h_{ao})$$

(2.1)

where $S_w^{II}(h_{aw})$ is the water saturation versus air-water capillary pressure function in the two phase air-water system, $S_w^{III}(h_{ow})$ is the water saturation function in the three fluid phase system, $S_t^{III}(h_{ao})$ is the total liquid saturation function for the three phase system, and β_{ao} and β_{ow} are scaling factors that depend on the interfacial tensions for the various fluid pairs (see Section 2.8). Combining (2.3) and (2.4) provides a general parametric form to describe three phase capillary pressure relations in terms of air-water capillary parameters and the two fluid-dependent scaling factors (*Parker et al.*, 1987).

2.3 Vertical Equilibrium Fluid Distributions

After a NAPL that has a specific gravity less than one reaches the water table, further vertical movement becomes limited by buoyancy forces. If vertical hydraulic gradients are small near the water table, vertical pressure distributions will approximate hydrostatic conditions. Deviations from true vertical equilibrium may be expected, especially in the unsaturated zone. However, these deviations may be accommodated by suitable definition of "quasi-static" capillary pressure relations, as discussed in Section 2.7.

Vertical equilibrium pressure distributions can be defined in terms of various fluid "table" elevations. In a monitoring well screened over an interval with free oil (Figure 2-6), one will observe an oil lens in the well that may be characterized by an air-oil table elevation, Z_{ao} (where the air-oil capillary pressure is zero), and an oil-water table elevation, Z_{ow} (where the oil-water capillary pressure is zero). One may also define an air-water table elevation, Z_{aw} (where air and water pressures are equal), which is related to the observed table elevations by

$$Z_{aw} = Z_{ow} + \rho_{ro} H_o$$

(2.5)

10

where $H_o=Z_{ao}-Z_{ow}$ is the apparent oil thickness or well hydrocarbon thickness. The vertical equilibrium capillary pressure distributions will be given by

$$h_{ao}=\rho_{ro}(Z-Z_{ao}) \tag{2.6a}$$

$$h_{ow}=(1-\rho_{ro})(Z-Z_{ow}) \tag{2.6b}$$

where Z is any elevation above the datum used to define table elevations. Stipulation of any two of the three table elevations completely defines the static three phase capillary pressure distributions. From the capillary pressure distributions and known or assumed saturation versus capillary pressure relations, vertical fluid distributions may be computed. Water saturation will be a function of oil-water capillary pressure, hence of height above Z_{ow}. Total liquid saturation will be a function of air-oil capillary pressure, hence of height above Z_{ao}. Using the three phase van Genuchten model of *Parker et al.* (1987), water and free oil saturations may be computed as

$$S_w=(1-S_m)(1+(\alpha\beta_{ow}h_{ow})^n)^{-m}+S_m \tag{2.7a}$$

$$S_o=(1-S_m)(1+(\alpha\beta_{ao}h_{ao})^n)^{-m}+S_m-S_w \tag{2.7b}$$

Vertical equilibrium water and oil saturation distributions for a representative case are shown in Figure 2-6. Note that oil saturation varies continuously with elevation and is not reasonably represented by a pancake-shaped distribution, contrary to common misconception (see Section 3.2). Field studies have indicated that the three phase van Genuchten model provides a good representation for both coarse and fine grained soils (*Huntley and Hawk*, 1992; *Ostendorf et al.*, 1993.)

11
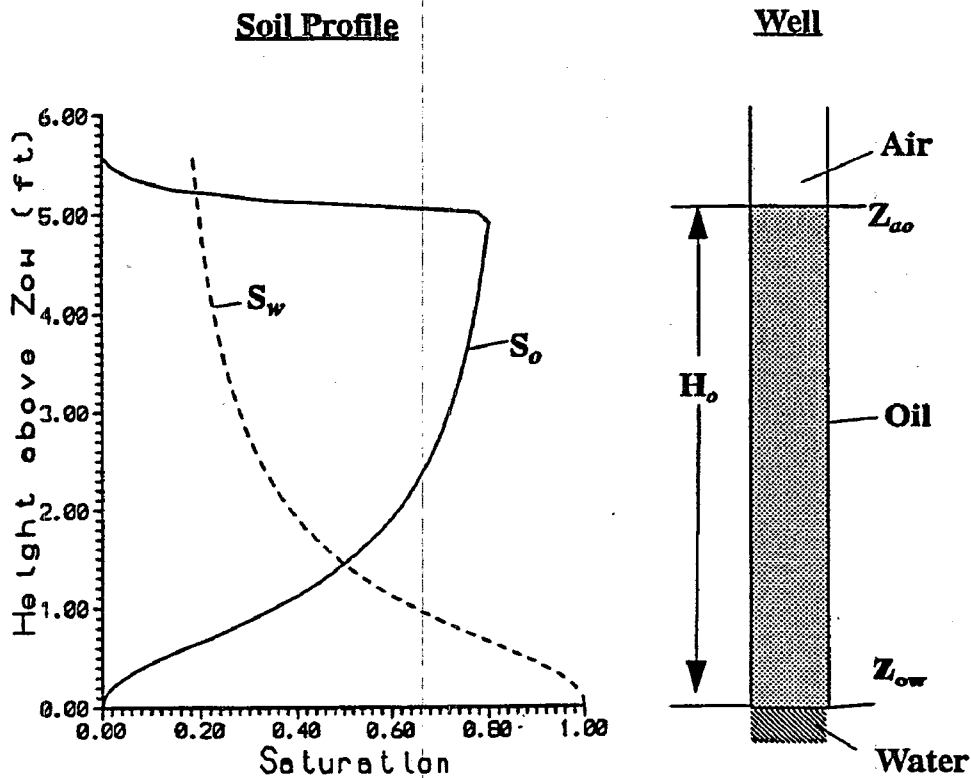
Figure 2-6. Three phase fluid distributions in equilibrium with a screened well.

Oil Specific Volume or "True Product Thickness"

The volume of free oil per unit area in the soil ("oil specific volume") may be computed by integrating the oil content over depth as

$$V_{of} = \int \phi S_{of} dZ \qquad (2.8)$$

where the limits of integration represent the upper and lower elevations where free oil occurs. The lower limit of integration is Z_{ow} and the upper limit may be computed as

$$(2.9)$$

$$Z_u = Z_{ow} + \frac{\rho_{ro}\beta_{ao}H_o}{\rho_{ro}\beta_{ao} - (1-\rho_{ro})\beta_{ow}}$$

12

Oil specific volume may be thought of as the "true oil thickness," in the sense that it is the thickness of product that would occur if all of the free oil over an area were extracted from the soil and placed in a container of same area. Employing (2.6), (2.7) and (2.8) will yield a relationship between V_{of} and H_o. Free oil specific volume versus well product thickness for gasoline in a sandy loam and typical silt loam soil (Table 2-3) is shown in Figure 2-7. Hysteresis in the capillary pressure relations will be manifested as hysteresis in the $V_{of}(H_o)$ function. Hysteresis in the curves is not shown, but some variations will occur during wetting and drainage paths. The functions illustrate the effects of a "capillary fringe" above the oil-water table, which results in a threshold apparent oil thickness before significant free oil occurs. The threshold for the sandy soil occurs between 0.5 to 1.0 feet, and for the silty soil it is about twice as great.
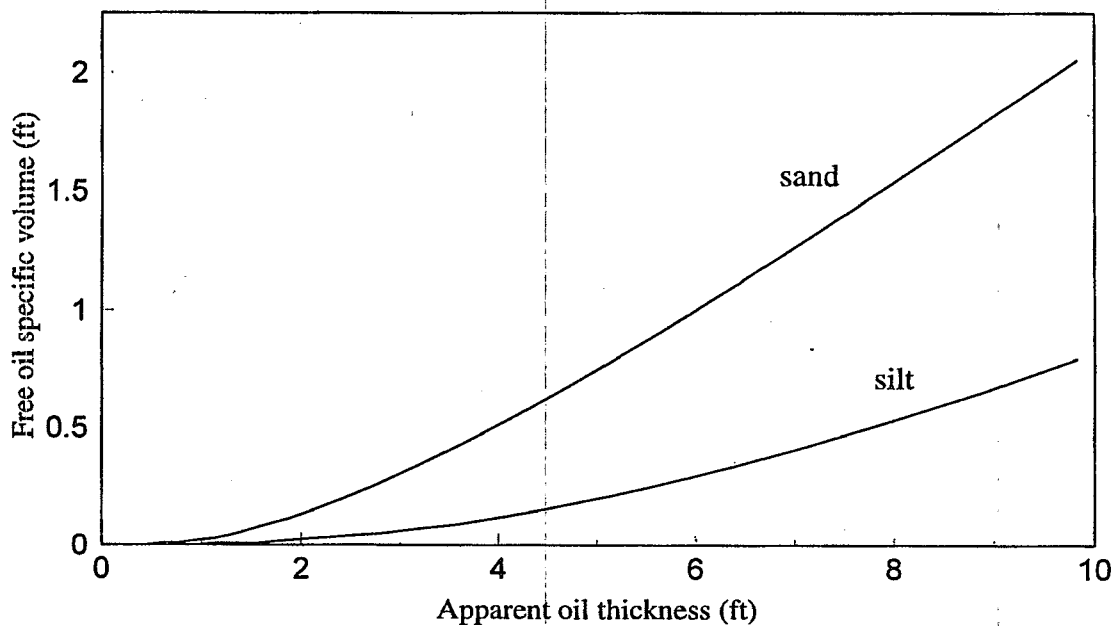
Figure 2-7. Free oil specific volume versus well oil thickness for gasoline in different soils.

13

2.4 Residual Oil in Saturated and Unsaturated Zones

Saturated Zone Residual Oil

When the oil-water table rises, oil-water capillary pressures decrease, resulting in increases in water saturation. Due to pore scale heterogeneities, water will displace oil from some pores faster than others, leaving islands of stranded oil, cut off from the continuous oil phase. This will result in "smearing" of the oil distribution below the zone of mobile phase hydrocarbon. At a given elevation, the *trapped oil saturation*, S_{ot}, may be calculated using the empirical model of *Land* (1968) as a function of the current water saturation, the historical minimum water saturation and the maximum residual oil saturation. The trapped oil specific volume may be computed by integrating the trapped oil specific volume as

$$V_{ot} = \int_{z_l}^{z_u} \phi S_{ot} \, dz$$

(2.10)

where S_{ot} is the trapped oil saturation that occurs as hydraulically discontinuous blobs occluded by the water phase. Since oil-water capillary head controls water saturation, it is evident that changes in the oil-water capillary head will govern oil entrapment, and that these changes will govern the trapped oil specific volume. Integration of (2.10) using Land's (1968) model indicates that trapped oil specific volume is of the form

$$dV_{ot} = \theta_{ot} dZ_{ow}$$

(2.11a)

where dV_{ot} is the change in trapped oil specific volume, dZ_{ow} is the increase in the oil-water table elevation above an elevation Z_{min} over a time interval, and θ_{ot} is the average incremental trapped oil content in the soil, which may be estimated as

$$\theta_{ot} = \min (\phi S_{or}, \overline{\theta}_{of})$$

(2.11b)

where S_{or} is the maximum residual oil saturation, and $\overline{\theta}_{of}$ is the average free oil content in the soil, approximated by

$$\overline{\theta}_{of} = \frac{V_{of}}{H_o}$$

(2.11c)

14

where V_{of} and H_o are the free oil specific volume and apparent product thickness, respectively. The elevation Z_{min} is given by

$$Z_{min}=Z^{ow}_{min}+Z_c \qquad (2.11d)$$

$$Z_c=\min\left(\frac{1}{2\alpha\beta_{ow}(1-\rho_{ro})},\frac{H_o}{3}\right) \qquad (2.11e)$$

where Z^{min}_{ow} is the historical minimum oil-water table elevation, and Z_c is the change in the oil-water capillary fringe thickness due to a reversal in wetting history from water drainage to water imbibition.

Unsaturated Zone Residual Oil

In addition to residual oil caused by fluid entrapment during water imbibition, another source of residual oil arises due to retention in the unsaturated zone. During periods of falling Z_{ao}, downward oil redistribution eventually becomes negligible under gravitational forces, as oil saturation reaches a critical value. We refer to this value as the *unsaturated zone residual saturation*. The increase in residual oil specific volume in the unsaturated zone due to an incremental drop in the air-oil table, ΔZ_{ao}, may be described by

$$\Delta V_{og}=\phi S'_{og}\Delta Z_{ao} \qquad (2.12)$$

where $S'_{og}= Min\ (S_{og},\overline{S}_o)$, in which S_{og} is the *maximum unsaturated zone residual saturation* after drainage from a high oil content, and $\overline{S}_o$ is the average free oil saturation at a given areal location.

Water Table Fluctuations

When water table fluctuations occur, the volume of residual product may increase and decrease over time as product becomes trapped or released. If fluctuations occur within a historical band, when the water table falls, the saturated zone residual decreases and the unsaturated zone residual increases. Usually the volume of product released from the saturated zone exceeds the volume tied up in the unsaturated zone, so the free oil specific volume increases. This results in an increase in apparent oil thickness that will be observed in monitoring wells (*Kemblowski and*

15

Chiang, 1990). When the water table rises, the converse will occur. Additional factors that tend to magnify the effect of water table fluctuations on apparent thickness include hysteresis in capillary pressure relations and nonequilibrium vertical pressure gradients.

2.5 Oil Relative Permeability and Transmissivity

Horizontal movement of free product at the water table is controlled by the oil piezometric gradient and the oil transmissivity given by the vertically integrated form of Darcy's law as

(2.13)

$$Q_o = -T_o \frac{\partial \Psi_o}{\partial x}$$

where Q_o is the vertically integrated oil flux $[L^2 T^{-1}]$, $\Psi_o = Z_{ao} + h_a/\rho_{ro}$ is the oil piezometric head in which Z_{ao} is the air-oil table and h_a is the air pressure in units of water height, ρ_{ro} is oil specific gravity, and T_o is the oil transmissivity defined by

(2.14)

$$T_o = \frac{\rho_{ro}}{\eta_{ro}} \int_{z.}^{z_u} k_{ro} K_{sw} dZ$$

where ρ_{ro} is the oil specific gravity, η_{ro} is the oil-water viscosity ratio, k_{ro} is the oil relative permeability, K_{sw} is the saturated hydraulic conductivity, and the limits of integration are the upper and lower elevation where free oil occurs.

Note that in the absence of a gas pressure gradient, oil flow occurs in response to a gradient in the air-oil table. If a gas pressure gradient occurs, its effect on oil flow will be additive with the air-oil table gradient.

Oil relative permeability increases with increasing water and oil contents and may be computed from the *van Genuchten* (1980) model with a refinement to correct for residual oil after *Kaluarachchi and Parker*. (1992) as

(2.15)

$$k_{ro} = (\overline{S}_t - \overline{S}_w)^{1/2} ((1 - \overline{S}_m^{1/m})^m - (1 - \overline{S}_t^{1/m})^m)^2$$

16

Where $\overline{S}_t = (S_w + S_{of} - S_m)/(1 - S_m)$ is effective total liquid saturation and $\overline{S}_w = (S_w - S_m)/(1 - S_m)$ is effective water saturation. Assuming vertical equilibrium fluid distributions, (2.14) may be integrated using (2.15) to obtain oil transmissivity as a function of free oil specific volume or apparent oil thickness for a given soil and for a given hydrocarbon. Oil transmissivity is nearly a linear function of free oil specific volume (Figure 2-8).
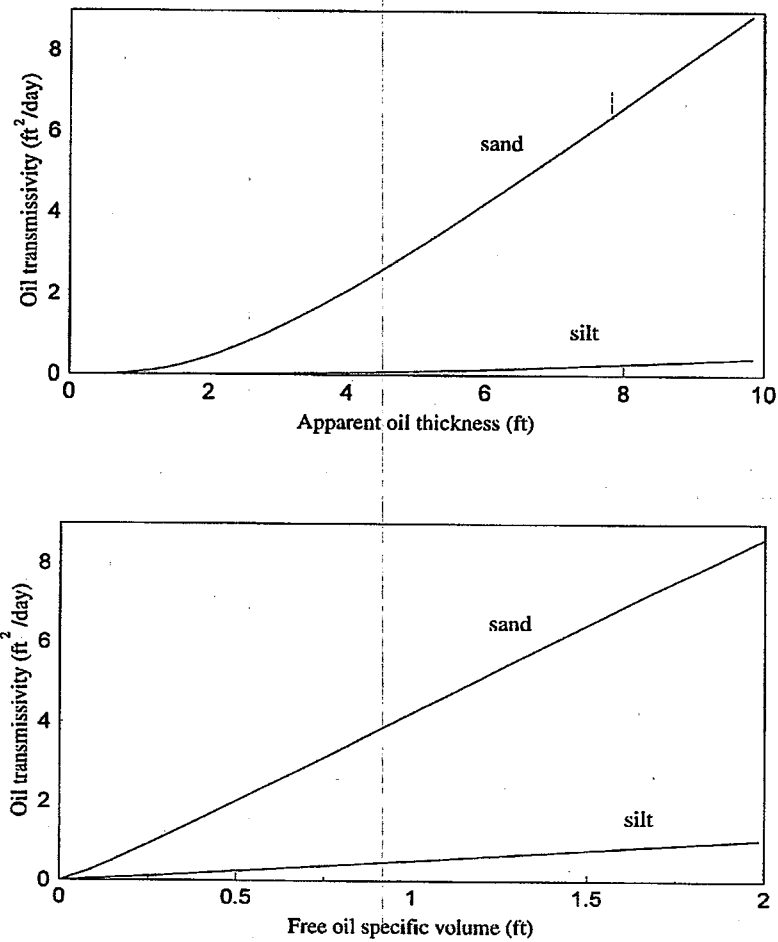
Figure 2-8. Typical oil transmissivity functions for gasoline in sandy and silty soils.

2.6 Estimation of Fluid Proterties

The following two sections summarize methods for estimating soil and fluid properties that govern NAPL retention and movement in the subsurface listed in Table 2-1.

Product Specific Gravity

Oil specific gravity, ρ_{ro}, varies significantly for different petroleum hydrocarbons depending on their chemical composition (Table 2-2). We recommend direct measurement of specific gravity, since such determinations are very simple and inexpensive to perform. Measurements may be performed in the laboratory on product samples using standard methods for fluid density determination. Since hydrocarbon density varies with temperature, measurements should be made at a temperature close to that expected in the field.

A simple field procedure to determine product density in wells with free product is to measure the water piezometric elevation (Z_{aw}) using a tube inserted through the oil layer in the monitoring well, and to measure the air-oil and oil-water table elevations under static conditions. We compute the product density by

$$\rho_{ro} = \frac{Z_{aw} - Z_{ow}}{Z_{ao} - Z_{ow}} \qquad (2.16)$$

Since (2.16) assumes that equilibrium conditions exist within the well bore, it is advisable to wait until fluid levels are stable after inserting piezimeter tubes before taking readings.

Product Viscosity

Dynamic (also called "intrinsic") viscosity can be measured using standard methods (e.g., ASTM D-88, D-4243, D-871, D-1795). For refined petroleum hydrocarbons, we have found the following approximate correlation between specific gravity and viscosity for various hydrocarbons

$$\eta_{ro} = 8.28 \rho_{ro}^{9.5} \qquad (2.17)$$

where η_{ro} is the ratio of dynamic viscosity of product to that of water.

18

Typical values for various products are given in Table 2-2 at 15 °C (*API,* 1989).. Viscosity increases with decreasing temperature by about 1-2 percent per degree Celsius.

Table 2-1. Soil and Fluid Properties for Three Phase Flow

Fluid properties:

ρ_{ro} Ratio of oil to water density $[L^0]$

η_{ro} Ratio of oil to water viscosity $[L^0]$

β_{ao} Ratio of water surface tension to oil surface tension $[L^0]$

β_{ow} Ratio of water surface tension to oil-water interfacial tension $[L^0]$

Soil properties:

K_{sw} Saturated hydraulic conductivity $[LT^{-1}]$

ϕ Total porosity $[L^0]$

S_m Water saturation at field capacity $[L^0]$

S_{og} Maximum unsaturated zone residual oil saturation $[L^0]$

S_{or} Maximum saturated zone residual oil saturation $[L^0]$

α VG pore size parameter $[L^{-1}]$

n VG pore size distriution exponent $[L^0]$

Table 2-2. Typical Specific Gravity ($R\rho_{ro}$), Oil-Water Viscosity Ratio ($H\eta_{ro}$), and Capillary Scaling Factors (βB_{ao} and $B\beta_{ow}$) for Various Hydrocarbon Mixtures

Product	ρ_{ro}	η_{ro}	β_{ao}	β_{ow}
Gasoline	0.73	0.45	3.5	1.4
Diesel fuel	0.83	2.7	2.2	1.9
Fuel oil #2	0.87	5.3	1.9	2.1
Fuel oil #5	0.92	215	1.6	2.8

Fluid Scaling Factors

Air-oil and oil-water scaling factors (β_{ao} and β_{ow}) are necessary to describe three phase saturation-capillary pressure relations. One may estimate the scaling factors from oil surface tension and oil-water interfacial tension date (*Lenhard and Parker,* 1987) as

$$\beta_{ao}=\sigma_w/\sigma_o \tag{2.18a}$$

$$\beta_{ow}=\sigma_w/\sigma_{ow} \tag{2.18b}$$

where σ_w is the surface tension of water (ca. 68 dynes/cm), σ_o is the surface tension of the organic liquid, and σ_{ow} is the oil-water interfacial tension. An alternative protocol for determining β_{ow} is to measure the surface tension of water saturated with dissolved hydrocarbon (in other words, water which has been shaken with hydrocarbon and decanted to remove all traces of free liquid) and to estimate the interfacial tension via

$$\sigma_{ow} = \sigma'_w - \sigma_o$$

where σ'_w is the surface tension of water saturated with dissolved hydrocarbon. In the absence of measurements of either σ_{ow} or σ'_w, we may obtain an estimated of β_{ow}, assuming $\sigma'_w \approx \sigma_w$, which indicates that

$$\beta_{ow} \approx \frac{1}{1 - 1/\beta_{ao}} \qquad (2.20)$$

Surface and interfacial tensions may be determined in the laboratory using standard methods (e.g., ASTM D-971). For unrefined petroleum hydrocarbons (that is, crude oil), scaling factors may be estimated using a correlation between oil surface tension and specific gravity given by *Baker and Swerdloff* (1956) as

$$\beta_{ao} = \frac{1}{1 - 1/2\rho_{ro}} \qquad (2.21a)$$

$$\beta_{ow} = 2\rho_{ro} \qquad (2.21b)$$

which provides a simple procedure for estimating scaling factors for unrefined hydrocarbons in the absence of additional information. *Lyman et al.* (1982) reviewed procedures for estimation of surface tension and interfacial tensions of fluid mixtures.

2.7 Estimation of Soil Properties

Soil properties required to describe oil and water retention and movement include parameters defining the fluid retention properties and soil permeability. If properties exhibit variations in the vertical direction, parameters relevant to the capillary fringe zone (where more oil occurs) should be used to predict oil recovery with maximum accuracy. If this results in an under- (or over-) estimate of the water transmissivity, one may correct it by adjusting the effective and

actual aquifer lower boundarier deeper (or shallower) in proportion to the error in the aquifer conductivity.

Pump tests or slug tests are the perferred method to obtain saturated hydraulic conductivity, although laboratory tests may be sufficiently accurate if sample disturbance is minimal and enough samples are obtained to compute a representative average. When averaging multiple determinations of hydraulic conductivity or other soil parameters, we recommend employing a geometric average as

(2.22)

$$G = \exp \left\{ \frac{\Sigma \ln X_i}{N} \right\}$$

where X_i are the measurements (i = 1,...,N) and G is the geometric average.

Total Porosity, Effective Porosity and Field Capacity

Total porosity, ϕ may be determined directly from soil cores, or indirectly from neutron logging or other in situ methods. The parameter S_m represents the minimum water saturation that will occur in the soil under field conditions. Note that the minimum saturation determined by fitting to laboratory moisture retention data is usually smaller than the minimum field water content, because equilibrium conditions do not occur in the field. We may estimate S_m from direct measurements of the degree of saturation on soil cores taken from the field at elevations above the "capillary fringe" where water saturation drops more or less sharply.

If the specific yield of the unconfined aquifer is known, this may be used to estimate S_m as

(2.23)

$$S_m = 1 - \phi_e / \phi$$

where ϕ is the total porosity of the soil, and ϕ_e is the specific yield or "effective porosity." Measured specific yields often increase with the duration of pump tests due to "delayed yield" effects. Since long term drainage is of concern here (mostly weeks to months), specific yields from short term pump tests may lead to overestimation of S_m.

If laboratory moisture retention data are available, we may make an estimate of S_m by evaluating the water saturation at an air-water capillary pressure head of ca. 100 to 300 cm, which is commonly regarded as an approximation of "field capacity."

Residual Oil Saturations

Maximum residual oil saturations in the unsaturated and saturated zones are needed tro estimate recoverable product. One may determine the maximum unsaturated zone residual oil saturation, S_{og}, in the laboratory by measuring the oil saturation in a soil core taken at a location where oil has been able to drain from a previous oil imbibition event for at least several days. Note that water and oil will not drain from a short column in the laboratory as it does in the field becuase the capillary pressure at the column boundary is zero. Typical values of S_{og} for field soils are in the range given by

$$ S_{og} \approx f_{og} S_m (1-S_m) \tag{2.24} $$

where f_{og} may range from 0.2 to 0.5 with a median of around 0.3. Fluids with higher viscosities and soils that are more heterogeneous with tend to have larger f_{og} values. Theoretical analyses indicate that residual saturation increases approximately proportional to the fourth root of product viscosity (i.e., $f_{og} \alpha \eta_{ro}^{1/4}$, where η_{ro} is the oil-water viscosity ratio).

One may determine the saturated zone residual oil saturation, S_{or}, by measuring the final oil saturation in an initially water saturated soil core subjected to oil flooding followed by water flooding. Typical values of S_{or} are given by

$$ S_{or} \approx f_{or} (1-S_m) \tag{2.25} $$

where f_{or} ranges from 0.2 to 0.5 with a median of about 0.3. Fluids with higher viscosities, and soils that are more heterogeneous, tend to have larger f_{or} values.

Capillary Pressure Parameters from Soil Cores

Air-water capillary pressure curves are often characterized by fitting model parameters (i.e., α, n, and S_m) to water content versus capillary pressure data obtained in the laboratory on soil cores (which yield *true equilibrium* parameters). However, in the field, equilibrium is never truly attained since low relative permeabilities impede fluid drainage as wetting phase saturations

23

diminish. To correct for the deviation from equilibrium conditions, we use *quasi-static* model parameters, which yield the correct water saturation distribution under field conditions when assuming a hydrostatic water pressure distribution. *Lenhard and Parker* (1990) describe procedures to estimate *quasi-static* retention parameters from laboratory data. The simplest approach is to fix S_m at a value corresponding to the minimum field saturation, discard moisture data below about $S_w \approx 1.1 \times S_m$, then fit the parameters α and n to the reduced data set using a nonlinear regression method. Table 2-3 gives typical quasi-static van Genuchten (VG) model parameters for various soil types computed from equilibrium values reported by *Carsel and Parish* (1988).

Table 2-3. Representative Soil Properties for Various Soils

Soil type*	K_{sw} (ft/d)	α (1/ft)	n	S_m	S_{or}	S_{og}
Sand	23.1	4.5	2.7	0.13	0.26	0.03
Loamy sand	11.5	3.8	2.4	0.21	0.24	0.05
Sandy loam	3.48	2.3	2.0	0.24	.0.23	0.05
Sandy clay loam	1.02	1.8	1.5	0.28	0.22	0.06
Loam	0.82	1.1	1.7	0.35	0.19	0.07
Silty loam	0.36	0.67	1.7	0.43	0.17	0.07
Clay loam	0.20	0.64	1.7	0.55	0.13	0.07
Sandy clay	0.095	0.97	1.8	0.66	0.10	0.07
Silty clay loam	0.056	0.37	1.9	0.68	0.10	0.06
Silt clay	0.016	0.26	2.8	0.84	0.05	0.04

* Size classes in the USDA classification system.

Capillary Pressure Parameters from Grain Size Data
Arya and Paris (1981) derived a theoretical procedure to estimate air-water capillary pressure parameters (that is, α, n, S_m) based on the proposition that capillary pressure relations relate to the pore size distribution of the soil, which we may in turn infer from the grain size distribution. *Mishra et al.* (1988) calibrated and implemented the method in the program SOILPROP (*ES&T*, 1990), which is also incorporated into the program SpillCAD (*ES&T*, 1994).

Capillary Pressure Parameters from Saturated Conductivity

Another method to estimate the VG parameter α is to employ a correlation with saturated hydraulic conductivity as

$$\alpha \approx A K_{sw}^{\frac{1}{2}} \qquad (2.26)$$

Based on laboratory analyses of vertical conductivity $A \approx 1.5 d^{\frac{1}{2}} ft^{-3/2} (\pm 50\%)$. Since field-measured horizontal conductivities (for example, from slug or pump tests) are generally much higher than vertical laboratory values, estimates of α using the foregoing value of A and field measured conductivities may be higher than values estimated from grain size distribution data. The true field parameter values probably lie between these estimates.

Capillary Pressure Parameters from Soil TPH Data

The most critical parameter in estimating oil saturation distributions and spill volume is generally the capillary curve parameter α. If independent data are available on oil saturation at points in the field, under certain conditions it may be possible to use these to calibrate the value of α. Since oil saturation and soil total petroleum hydrocarbon (TPH) are related, methods may be developed to calibrate α from TPH and monitoring well data. The method is based on the premise that oil saturation distributions computed for given well fluid levels, from the three phase saturation relations discussed in Section 2.3, should agree with TPH data, if fluid levels at the time soil samples are taken are known and if one properly calibrates the capillary model. Required data to employ this strategy include well product thickness (H_o) and oil-water table elevations (Z_{ow}) in monitoring wells at specified coordinates (x_w, y_w), TPH measurements from a given depth interval for specified coordinates (x_T, y_T), as well as estimates of total porosity (ϕ), irreducible water saturation (S_m), the van Genuchten parameter (n), oil specific gravity (ρ_{ro}), and fluid scaling factors (β_{ao} and β_{ow})

The major steps of the algorithm are as follows: (i) interpolate Z_{ow} and H_o at locations (x_T, y_T), where TPH is measured onto a regular computational grid, (ii) at each soil bore location, calculate an average oil saturation $\overline{S}_o$ from the interpolated fluid levels over the interval of TPH measurements, and use this $\overline{S}_o$ to calculate a corresponding TPH value, (iii) compare measured and calculated TPH values and iteratively adjust the value of α to minimize the sums of squared deviations.

Free oil saturation S_{of} at a given location (x_t, y_t) and elevation Z is computed as described in Section 2.3, and $\overline{S}_o$ is determined by averaging S_o computed at midpoints, lower and upper limits for TPH measurement intervals. TPH (in mg/kg) is calculated from $\overline{S}_o$ as

$$TPH = \frac{\rho_o \overline{S}_o \phi}{\rho_b} \times 10^6$$

where ρ_o is the oil density and ρ_b is the soil bulk density.

The applicability of this method is critically dependent on accurately defining the fluid levels at the time TPH samples are taken. The method will be most reliable if well product thickness is large (several feet), because uncertainty in fluid levels will have less effect on TPH predictions. The difficulty of making accurate measurements of TPH in the zone of free product should be carefully considered in employing this method.

Section 3

Spill Assessment Methods

3.1 Interpretation of Soil Concentration Data

If measurements of soil total petroleum hydrocarbon (TPH) are available at a sufficient number of points in space to accurately define a three-dimensional distribution of NAPL in the subsurface, hydrocarbon volume estimation is straightforward. We simply interpolate the hydrocarbon content in space and perform the volume integration. However, three-dimensional interpolation is computationally intensive and requires a high density of sampling points to justify its use. To minimize these difficulties, a two-step integration procedure may be used, which is more efficient and robust with sparse data sets. The procedure involves (I) vertical integration of oil content using linear interpolation between measurement depths, followed by (ii) areal interpolation and integration using a two-dimensional kriging algorithm.

Determination of soil TPH involves extraction of soil samples and analytical quantification of hydrocarbons in terms of mass of hydrocarbon per mass of dry soil. TPH extractions yield hydrocarbon mass present as a nonaqueous phase liquid, as dissolved components in the aqueous phase, as adsorbed components, and as components in the gas phase (to the extent they are not lost during sample processing). Calculations based on equilibrium partitioning indicate that when a nonaqueous phase exists in a sample, the majority of the hydrocarbon mass is in the separate phase, unless the natural organic content of the soil is high. Therefore, estimating nonaqueous phase volume directly from TPH incurs a very small error. In practice, interpolation and measurement errors are much greater.

The volumetric oil content, θ_o, which is the volume of oil per volume of soil, is related to TPH by

(3.1)

$$\theta_o = \frac{\rho_b TPH}{\rho_o 10^6}.$$

where ρ_b is the soil bulk density $[ML^{-3}]$, ρ_o is the oil density $[ML^{-3}]$, and TPH is expressed in mg/kg. SpillCAD estimates bulk density as $\rho_s(1-\phi)$, where ϕ is soil porosity, and ρ_s is particle

density, which is generally between 2.6 and 3.0 g cm^{-3} (the density of quartz which is 2.65 g cm^{-3} is often assumed).

For a given bore hole, in which TPH measurements are available at various depths, we may compute the oil volume per unit horizontal area, or *oil specific volume*, V_o, by integrating the volumetric oil content over the vertical dimension as

$$V_o = \int_{z_l}^{z_u} \theta_o dZ \tag{3.2}$$

where z_l and z_u are the lower and upper elevations where oil occurs (or the range over which we are interested in estimating product volume). The integration may be readily carried out numerically by linearly interpolating oil contents between measurement points along the vertical dimension.

Oil specific volume computed from (3.2) for each soil boring may then be interpolated over a specified areal domain to obtain values of oil specific volume at N locations on a regular grid (for example, 20 x 20 nodes), with block dimensions $\Delta x \times \Delta y$ using a kriging algorithm, yielding N values of specific volume, V_{oi}, where I = 1,2,...,N. The total hydrocarbon volume, $\sum_o$, within the horizontal limits of the areal domain and within the vertical limits of the TPH sampling elevations is computed as

$$\sum_o = A \sum_{i=1}^{N} V_{oi} \tag{3.3}$$

where $A = \Delta x \Delta y$ is the grid block area. If TPH data are restricted to the unsaturated zone, then the estimated volume represents only the product in the unsaturated zone. Likewise, if the computational domain is limited to a subregion or TPH data are used for a limited depth range, the computed volume represents an estimate of the volume within a subregion.

Note that the hydrocarbon volume estimated from soil TPH data represents both free (i.e., mobile) and residual (i.e., immobile) hydrocarbon to the extent that both occur in soil samples. Samples taken in the unsaturated zone may represent primarily residual oil, whereas samples at the water table may be mostly free product-- although sampling within the zone of free product is not very reliable.

28

Estimating the Mass of a Component

If soil concentrations of specific components (for example, BTEX) are available, we may use the same procedure described above for total hydrocarbon to estimate the total mass of a measured component in the soil. If the soil concentration of species α, expressed in mg/kg, is Y_α, then we may compute the mass of α per area in the soil from the vertical distribution of Y_α in a bore hole as

(3.4)

$$m_\alpha = \int_{z_l}^{z_u} \frac{\rho_b Y_\alpha}{10^6} dz$$

where z_l and z_u are the lower and upper elevations where the contamination occurs (or the range over which we want to estimate species mass). Integration limits are the maximum and minimum elevations at which soil concentration measurements are available for a given bore hole. Integration of (3.4) may be performed numerically using piecewise linear interpolation between measurement elevations.

Values of the contaminant mass per area, m_α, computed at soil boring locations from (3.4) may be interpolated over a specified areal domain to obtain values at *locations* on a regular grid (for example, 20 x 20 nodes), using a kriging algorithm. We may then compute the total mass of species within the indicated domain as

(3.5)

$$M_\alpha = A \sum_{i=1}^{N} m_{ai}$$

where $A = \Delta x \Delta y$ is the grid block area, N is the number of nodes, and m_{α_i} is the mass of contaminant per area at node I.

Estimating the Volume of Contaminated Soil

When soil excavation or *ex situ* treatment of contaminated soil is being considered, the volume of contaminated soil must be estimated. The first problem then is to define operationally what is meant by "contaminated." This is typically either mandated by regulations or subject to negotiation with regulatory agencies based on risk assessment studies. We assume that the definition of "contaminated" is that the soil concentration for TPH, or for a given species (for example, benzene or total BTEX), exceeds a specified threshold value and that soil is considered to be "contaminated" if the soil concentration of interest, Y, is greater than Y_{crit}.

Using values of Y that are linearly interpolated between sampled elevations in the vertical direction as described above, we may define an indicator function as

$$\delta(z) = \begin{cases} 0 & \text{if } Y \leq Y_{crit} \\ 1 & \text{if } Y > Y_{crit} \end{cases}$$

<div align="right">(3.6)</div>

The volume of contaminated soil per area at soil boring locations is computed as

<div align="right">(3.7)</div>

$$L = \int_{z_l}^{z_u} \delta(Z) dZ$$

where z_l and z_u are the lower and upper elevations we specify. The L values are computed over a specified areal domain to obtain values at N nodes on a regular grid (for example, 20 x 20 nodes) using a kriging algorithm. We may then compute the volume of soil with concentration exceeding the threshold by

<div align="right">(3.8)</div>

$$V_{soil} = A \sum_{i=1}^{N} L_i$$

where $A = \Delta x \Delta y$ is the grid block area, N is the number of nodes, and L_i is the nodal value of L.

Example Calculations

To illustrate the calculations discussed above, soil concentration data for samples taken from a soil boring to a depth of 45 feet are used to compute total hydrocarbon specific volume, benzene mass per area, and volume of soil per area with TPH greater than 1000 mg/kg in a spreadsheet format given in Table 3-1. Given multiple soil borings, similar calculations may be repeated for other locations and the results interpolated over a spatial domain to determine total hydrocarbon volume, benzene mass and contaminated soil volume within the sampled region using (3.8). Interpolation may be carried out using commercial or public domain software (e.g., GEO-EAS or on a regular grid Surfer). The soil under consideration is assumed to have a porosity of 0.35 and a bulk density of 1.72 g/cm^3. The hydrocarbon density is assumed to be 0.80 g/cm^3. Values in Table 3-1 were computed as follows:

> Column A. Sample depth is the distance from the ground surface to the center of the core sample.

> Column B. The sample interval, dZ, is half the distance from the current sample to the next shallower sample, plus half the distance from the current sample to the next deeper sample, except for the shallowest and deepest samples, in which case, the interval is half the distance from the sample center to the next sample, plus 0.5 ft to account for one half of the actual length of the sample core.

Column C. Measured TPH in the soil core given as mg hydrocarbon per kg dry soil.

Column D. The average volumetric oil content in the sample interval computed from (3.1).

Column E. Each entry in the column is calculated as $\theta_o dZ$, and the entire column is summed to obtain the oil specific volume, $V_o = 0.206$ ft^3 per ft^2.

Column F. Measured soil benzene concentration expressed as mg benzene per kg dry soil.

Column G. The average benzene mass per area in g/ft^2 in the sample interval is computed from eq. (3.4), and the factor $f = 0.0283$ is inserted to make the proper unit conversions. The column is summed to obtain the mass of benzene per area over the boring depth, $m_{benz} = 39.8$ g/ft^2.

Column H. An indicator variable that is 1 if TPH$\leq$1000 mg/kg and 0 if TPH is smaller.

Column I. The volume of contaminated soil per area in each sample interval is calculated as $\delta(Z)dZ$. The column is summed to obtain the contaminated soil volume of 22.5 ft^3 per ft^2.

Table 3-1. Example Spreadsheet Calculations From Soil Boring Data

A	B	C	D	E	F	G	H	I
Depth (ft)	dZ (ft)	TPH (mg/kg)	θ_o (-)	V_o (ft^3/ft)	Y_α (mg/kg)	$f\rho_b Y_\alpha$ (g/ft^2)	$\delta(Z)$ (-)	$\delta(Z)dZ$ (ft^3/ft^2)
5	5.5	542	0.0012	0.006	5	1.3	0	0.0
15	8.0	1180	0.0025	0.020	9	3.5	1	8.0
21	6.5	3937	0.0085	0.055	37	11.7	1	6.5
28	8.0	6836	0.0147	0.118	53	20.7	1	8.0
37	8.5	678	0.0015	0.012	6	2.5	0	0.0
45	4.5	27	0.0001	0.000	0	1.2	0	0.000
				0.206		39.8		22.5

3.2 Free Oil Volume From Monitoring Well Data

Description of Method

As discussed in Section 2.3, free oil specific volume may be computed from well product thickness data, if vertical equilibrium pressure distributions are assumed and soil capillary pressure relations can be estimated. Areal integration of oil specific volume values will then provide an estimate of free oil volume over the areal domain.

The procedure that is recommended for performing these calculations begins with a set of well product thickness data for a given point in time from a monitoring well network. Well product thickness values (H_o) are interpolated aerially using a 2-D kriging algorithm to obtain estimates of H_o on a regular grid overlaying the site area. After interpolating well product thickness, the free oil specific volume, V_{of}, may be computed as described in Section 2.3 for each node. The total free product volume is then determined by summing over the area as

$$\Sigma_{of} = A \sum_{i=1}^{N} V_{of_i}$$

(3.9)

where $A = \Delta x \Delta y$ is the grid block area, N is the number of nodes in the grid, and V_{of_i} is the free oil specific volume at node I.

In addition to wells within the liquid hydrocarbon plume, enough wells should be available beyond the plume to define its perimeter. If sufficient wells do not exist to adequately delineate the plume, it may be necessary to define "control points" with zero oil thickness at locations dictated by professional judgment, rather than to rely on an *interpolating* algorithm to *extrapolate* the data.

An important consideration in computing product volume from well product thickness data is the validity of the assumption of equilibrium between the well and the surrounding soil as well as the assumption of vertical equilibrium in the soil. Under conditions in which an upward hydraulic gradient exists, oil specific volume computed assuming vertical equilibrium conditions may underestimate the actual free oil specific volume. With a downward gradient, oil specific volume may be overestimated.

If a well was recently installed or bailed, fluid levels will take some time to equilibrate between the soil and the well. How long this will actually take depends on the oil transmissivity, which will in turn depend on the soil and fluid properties as discussed in Section 2.5. The equilibration time may be determined in the field by monitoring well recovery versus time after bailing a well. A rough estimate of the equilibration time in days may be taken as $T_o^{-\frac{1}{2}}$ where T_o is the oil transmissivity in square feet per day computed per Section 2.5 as a function of soil and fluid properties and equilibrium well product thickness. For commonly encountered conditions, the well equilibration time may range from minutes to weeks. When wells have been bailed and

deviations from vertical equilibrium conditions are suspected, it may be better to employ the maximum product thickness at each well to compute spill volume rather than a time-synchronous data set.

Since well product thickness only reflects *free oil* under the existing hydraulic conditions, the computed spill volume is only an estimate of the free oil volume corresponding to the specified product level data. Historical changes in air-oil and oil-water table elevations can induce some oil to become hydraulically discontinuous and hence non-detectable by monitoring wells. This may cause computed free oil volumes to fluctuate over time with the occlusion or release of residual oil.

Evaluation of the "Oil Pancake" Approximation

A common conceptualization of the vertical distribution of free product at the water table is based on the idea that oil occurs as a distinct lens in which the drainable pore space is saturated with oil. This is often referred to as the "oil pancake." According to the general theory of capillary retention discussed in Section 2, such a step function fluid distribution in the soil will be approached only if the soil pores are very large so capillarity is negligible (*i.e.*, high value of van Genuchten α) or if the pore size distribution is very narrow (*i.e.*, high value of van Genuchten n). The oil pancake model is often employed to interpret baildown tests (*Gruszcenski*, 1987). In a baildown test, accumulated product in a monitoring well is bailed out over a short period of time and the response of the air-oil and oil-water interfaces in the well are recorded over time (Figure 3-1). The rate of oil flow into the well is controlled by the oil transmissivity and the air-oil head difference between the soil and the well. Water flow is controlled by the water transmissivity and the air-water (i.e., "corrected water table") head difference. During the initial stage of a baildown test, water and oil flow into the well in response to gradients in the air-water and air-oil tables, respectively. Since water transmissivity is usually much greater than oil transmissivity, water reaches an equilibrium condition earlier than the oil. As further oil flows into the well, the air-water table gradient is reversed and water is displaced from the well. According to the oil pancake model, the product thickness in the well when water flow reverses (oil-water table reaches a maximum) corresponds to the "formation product thickness" which is multiplied by the effective porosity to determine oil specific volume, often referred to as "true product thickness" in this context.

An analysis of baildown test results with the numerical model ARMOS was reported by *Zhu et al.* (1993). Well hydrographs for baildown tests with 2 feet of diesel fuel initially present in a monitoring well are shown in Figure 3-2 for two soils. For the sandy aquifer, the oil-water table peaks within one minute, while water flow into the well is still occurring after 30 minutes for the silty soil. A comparison of the oil saturation distribution inferred by the oil pancake model and the profile computed from the van Genuchten capillary model is shown in Figure 3-3 for the two tests. It is evident that the pancake model is not a very good approximation of the oil saturation distribution. Inspection of the area under the oil pancake and van Genuchten curves, which relate directly to the oil specific volume, indicates that the oil pancake model yields an estimate of oil specific volume that is within 10 percent of the actual volume for the sandy soil.

33

For the silty soil, the oil pancake model overestimates oil specific volume by a factor of 2.5 to 4.0, depending on the coarseness of the filter pack material. Oil drainage from the filter pack after bailing is misinterpreted as recovery from the formation by the oil pancake model.

The results indicate that the oil pancake model provides a poor approximation of the free oil distribution and leads to erroneous estimates of free oil volume. Overestimation of free oil specific volume will be increasingly severe for finer grained materials. Quantitative determination of oil transmissivity and oil specific volume from baildown tests requires consideration of transient two phase oil-water flow using an appropriate numerical model.
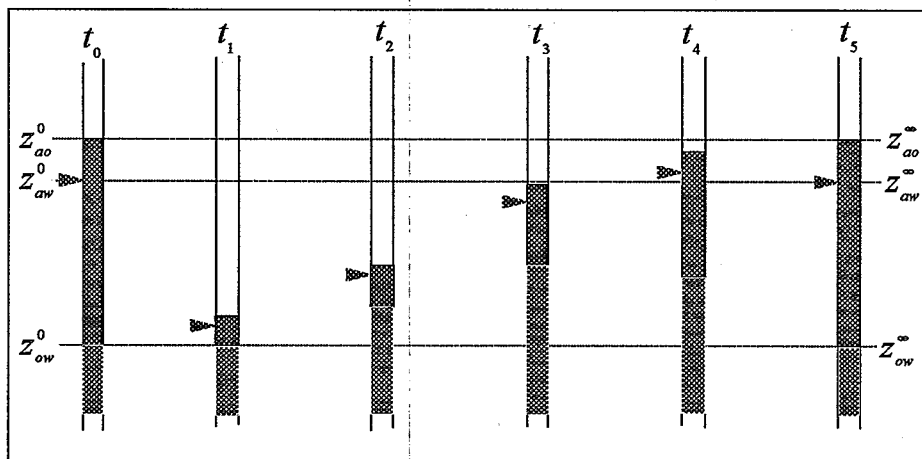
Figure 3-1. Schematic of baildown test over time.
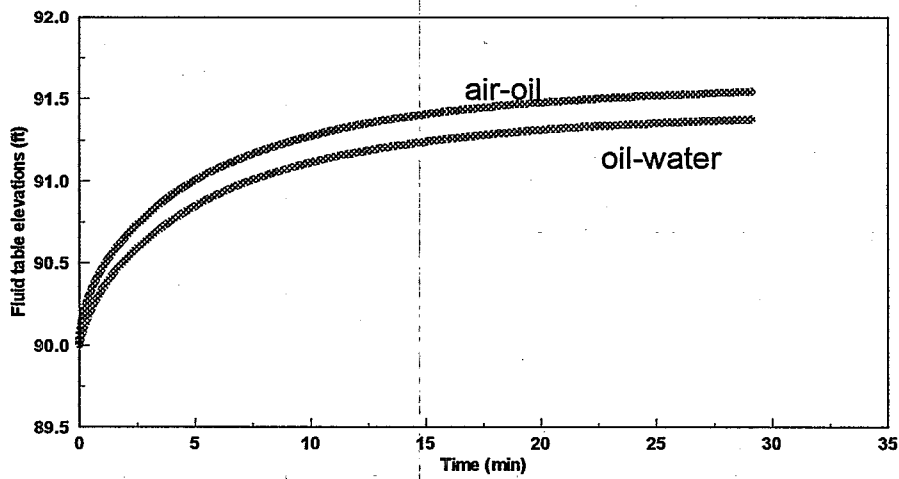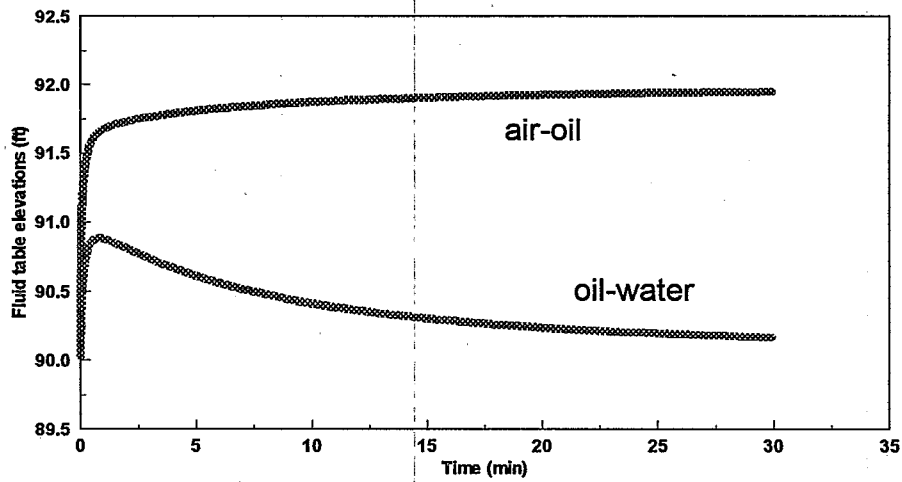
Figure 3-2. Baildown test hydrograph for a) sandy soil and b) silty soil with diesel.
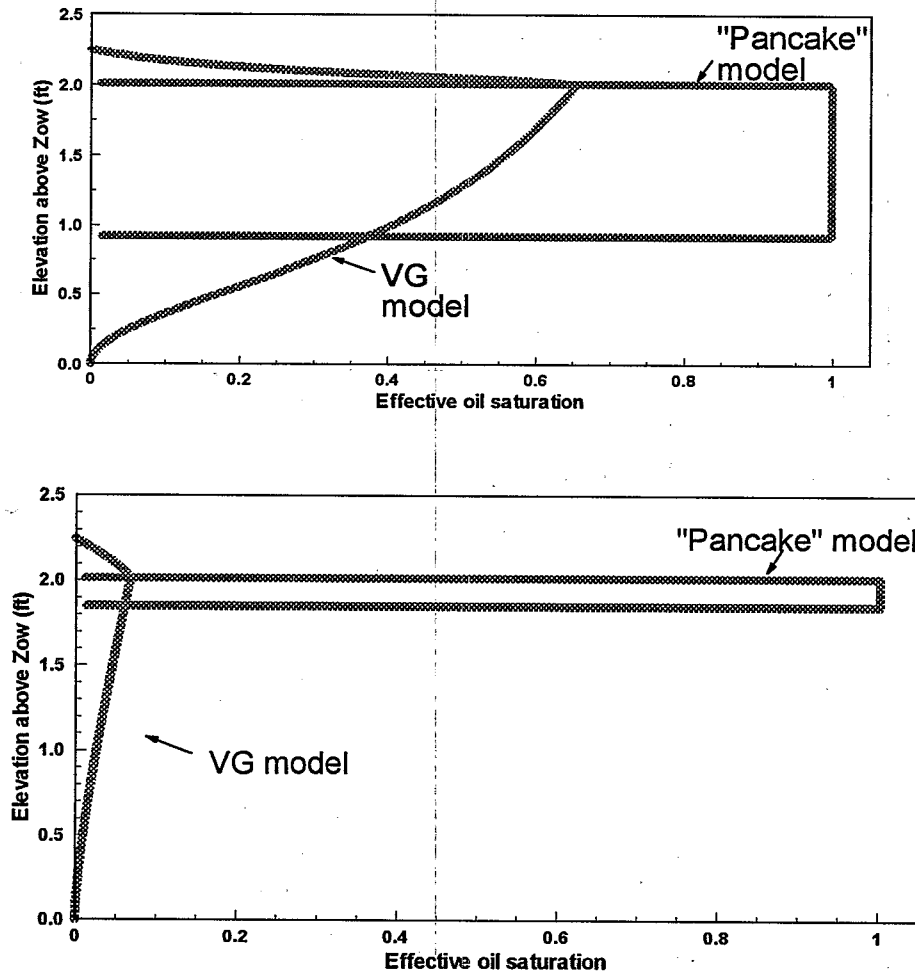
Figure 3-3. Oil saturation distribution for van Genuchten model and "oil pancake" model for a) sandy soil with diesel and b) silty soil with diesel.

Example Calculations

An example calculation is shown in spreadsheet form to compute free oil specific volume, V_{of}, from well product thickness, H_o, in a monitoring well. The well product thickness for the example is 3 feet and the air-oil and oil-water table elevations are 93 and 90 feet, respectively. Assumed soil and fluid properties for the problem are given in Table 3-2. Vertical integration is performed from a lower elevation of Z_{ow}=90 feet to an upper elevation of Z_u=93.4 feet, computed from (2.9). Calculations are performed at 35 equal depth intervals of 0.1 feet to numerically integrate for oil specific volume. To compute total free oil volume, calculations of oil specific volume must be repeated at various areal locations. Since well product thickness must be

a smooth function in space (discontinuities in the piezometric gradients cannot occur), while oil specific volume may be discontinuous due to soil heterogeneity, it is preferable to interpolate H_o from monitoring wells onto a computational grid and to compute V_{of} on the grid from interpolated apparent thickness values. Values in Table 6 were computed as follows:

Column A. The first value of Z is Z_u from (2.9), the final value is Z_{ow}, and intermediate values are incremented in intervals of dZ=0.1 ft.

Column B. The oil-water capillary pressure h_{ow} is calculated as .

$$h_{ow}=(1-\rho_{ro})(Z-Z_{ow})$$

Column C. Air-oil capillary pressure is calculated using eq. (2.6a) above Z_{ao}. At lower elevations h_{ao}=0 is employed to compute total liquid saturation.

Column D. Water saturation is calculated using eq. (2.7a) given h_{ow} at the specific depth.

Column E. Free oil saturation is calculated for each depth as $S_{of}=S_t-S_w$.

Column F. The free oil volume per unit area for each depth interval is computed as $\phi S_{of}dZ$. A sum of all values in column F gives the free oil specific volume of 0.309 ft^3/ft^2.

Table 3-2. Soil and Fluid Properties for Example Problem.

ρ_{ro}=0.8	K_{sw}=8.0 ft day^{-1}	S_m=0.15
η_{ro}=0.6	$\phi = 0.35$	S_{og}=0.06
β_{ao}=3.2	α=2.5 ft^{-1}	S_{or}=0.20
β_{ow}=1.5	n=2.0	

Table 3-3. Spreadsheet for Free Oil Specific Volume from Well Product Thickness

A	B	C	D	E	F
Z (ft)	h_{ow} (ft)	h_{ao} (ft)	S_w (-)	S_{of} (-)	$\phi S_{of} dZ$ (ft^3/ft^2)
93.4	0.68	0.32	0.46	0.00	0.000
93.3	0.66	0.24	0.47	0.08	0.003
93.2	0.64	0.16	0.48	0.20	0.007
93.1	0.62	0.08	0.49	0.38	0.013
93.0	0.60	0.00	0.50	0.50	0.018
92.9	0.58	0.00	0.51	0.49	0.017
92.8	0.56	0.00	0.52	0.48	0.017
92.7	0.54	0.00	0.53	0.47	0.017
92.6	0.52	0.00	0.54	0.46	0.016
92.5	0.50	0.00	0.55	0.45	0.016
92.4	0.48	0.00	0.56	0.44	0.015
92.3	0.46	0.00	0.58	0.42	0.015
92.2	0.44	0.00	0.59	0.41	0.014
92.1	0.42	0.00	0.61	0.39	0.014
92.0	0.40	0.00	0.62	0.38	0.013
91.9	0.38	0.00	0.64	0.36	0.013
91.8	0.36	0.00	0.66	0.34	0.012
91.7	0.34	0.00	0.67	0.33	0.011
91.6	0.32	0.00	0.69	0.31	0.011
91.5	0.30	0.00	0.72	0.28	0.010
91.4	0.28	0.00	0.74	0.26	0.009
91.3	0.26	0.00	0.76	0.24	0.008
91.2	0.24	0.00	0.78	0.22	0.008
91.1	0.22	0.00	0.81	0.19	0.007
91.0	0.20	0.00	0.83	0.17	0.006
90.9	0.18	0.00	0.85	0.15	0.005
90.8	0.16	0.00	0.88	0.12	0.004
90.7	0.14	0.00	0.90	0.10	0.003
90.6	0.12	0.00	0.93	0.07	0.003
90.5	0.10	0.00	0.95	0.05	0.002
90.4	0.08	0.00	0.96	0.04	0.001
90.3	0.06	0.00	0.98	0.02	0.001
90.2	0.04	0.00	0.99	0.01	0.000
90.1	0.02	0.00	1.00	0.00	0.000
90.0	0.00	0.00	1.00	0.00	0.000
					0.309

3.3 Estimation of Dissolved and Free Phase Travel

Description of Method

In order to assess the potential for adverse impacts of a hydrocarbon spill, it is often useful to estimate the migration rates of dissolved and free phase plumes. These can be used in turn to estimate travel times to property boundaries or potential receptor locations (e.g., wells, streams, etc.). The average velocity of a dissolved phase plume, v_w, is given by

$$v_w = \frac{q_w}{R\phi} = \frac{K_{sw}}{R\phi} \frac{dZ_{aw}}{dx}$$

(3.10)

where q_w is the Darcy velocity for water, ϕ is porosity, R is a retardation factor accounting for adsorption, K_{sw} is the saturated hydraulic conductivity, and dZ_{aw}/dx is the corrected water table gradient. Use of total porosity in (3.10) assumes that all pore space is accessible to dissolved contaminant. A retardation factor of 1.0, which corresponds to no adsorption, represents the worst case with regard to dissolved plume migration -- i.e., maximum migration rate.

The average velocity of the free phase hydrocarbon plume, v_o, is given by

$$v_o = \frac{q_o}{\phi S_o} = \frac{T_o}{V_{of}} \frac{dZ_{ao}}{dx}$$

(3.11)

where q_o is the Darcy velocity for oil, ϕ is porosity, S_o is the oil saturation, T_o is the oil transmissivity, V_{of} is the free oil specific volume, and dZ_{ao}/dx is the air-oil table gradient. The relationship between the mobility factor, $M_o = T_o/V_{of}$, and apparent oil thickness, H_o, may be determined from the functions discussed in Sections 2.3 and 2.5. The results indicate that the mobility factor increases with H_o up to a maximum value given by

$$M_o^{max} = \frac{\rho_{ro} K_{sw}}{\eta_{ro} \phi (1 - S_m)}$$

(3.12)

where ρ_{ro} is the oil specific gravity, η_{ro} is the oil-water viscosity ratio, K_{sw} is the soil hydraulic conductivity, ϕ is total porosity and S_m is the residual water saturation.

Variations in the mobility factor with H_o are illustrated in Figure 3-4, which shows the relative mobility factor, M_o/M_o^{max}, for a sandy and a silty soil. For the sandy soil, the mobility reaches a maximum between 5 to 10 feet. For the silty soil, a maximum value is reached at an apparent oil thickness of about 15 feet. If M_o/M_o^{max} is used to estimate oil plume velocity, the results will tend to overestimate the movement on the perimeter of the plume where the mobility factor diminishes. Figure 2-7 indicates that the minimum apparent thickness for the same sandy

39

and silty soils due to capillary exclusion are approximately 1 and 2 feet, respectively. Inspection of Figure 3-4 indicates that the oil relative mobility for both soils is approximately 0.5 at their respective minimum apparent thickness values. Therefore, the oil mobility factor on the plume perimeter should be approximately half of the maximum value given by (3.12).
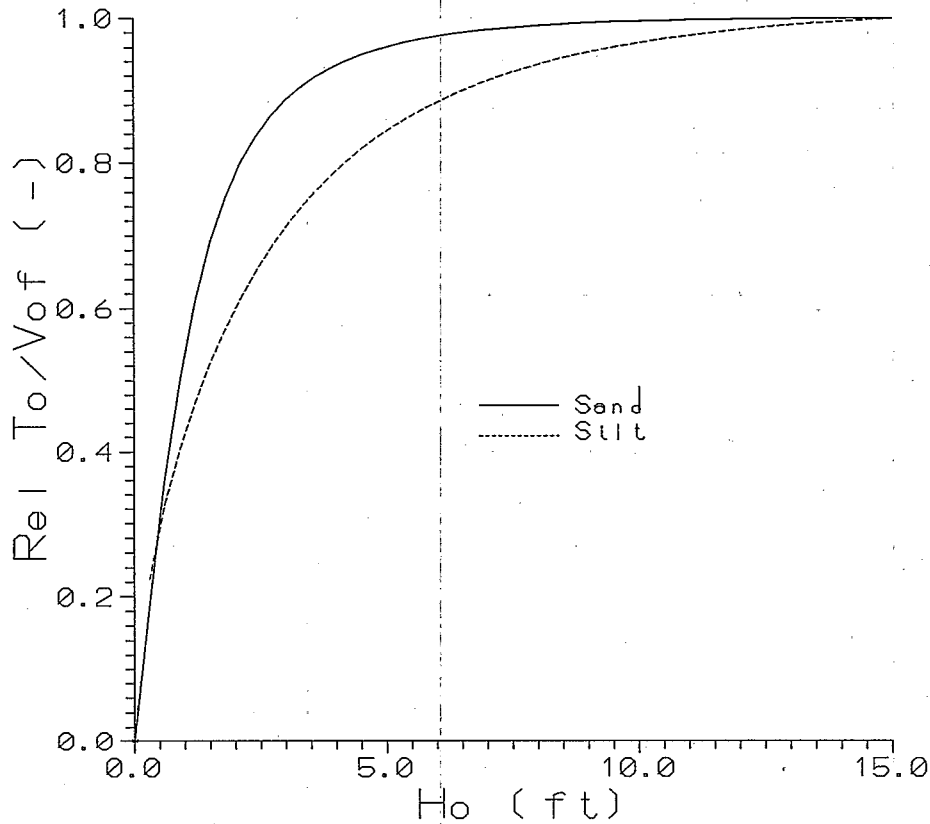
Figure 3-4. Relative oil mobility versus apparent oil thickness for two soils.

The time for a dissolved or free phase plume to travel a distance along a streamline may be computed as

(3.13)

$$\Delta t = \frac{\Delta x}{v_p}$$

where v_p is the velocity of phase p (i.e., oil or water). The distance must be measured along a path perpendicular to the potential contours, which correspond to the air-water table for water flow or the air-oil table for oil flow in the absence of air pressure gradients. If the gradients change significantly along a streamline, the travel time calculations are performed along intervals

40

for which the gradient can be approximated as constant, and travel times for the increments are then added.

Example Calculations

The foregoing algorithm for estimating free phase plume migration rate was evaluated by comparing analytical results with those of the numerical model ARMOS for transient water and NAPL flow (*ES&T*, 1994). The problem involves a 54,000 gallon gasoline leak in an aquifer with a 0.5 percent regional water table gradient. Relevant soil and fluid properties are shown in Table 3-2.

The distribution of the apparent oil thickness 100 days after the gasoline leak is repaired and 700 days after the leak is repaired, as predicted by the numerical model, is shown in Figure 3-5. Over the 600 day period, the outer edge of the free phase plume (taken operationally as the 0.25 ft apparent thickness contour) has migrated about 50 feet, indicating an average oil plume velocity v_o of 0.083 feet per day.

To estimate the free phase plume velocity with the analytical model, we first compute the mobility factor for the gasoline plume as

$$(3.14)$$

$$M_o \approx \frac{M_o^{max}}{2} = \frac{\rho_{ro} K_{sw}}{2\eta_{ro} \phi (1-S_m)} = 17.9 \text{ ft/day}$$

The average oil piezometric gradient (air-oil table) will be roughly equal to the water piezometric gradient (air-water table), which is 0.5 percent. The maximum free phase plume velocity may be estimated as

$$(3.15)$$

$$v_o \cong M_o \frac{dZ_{aw}}{dx} = 0.09 \text{ ft/day}$$

The estimated oil velocity of 0.09 feet is approximately equal to the value of 0.083 feet per day indicated by the numerical model.
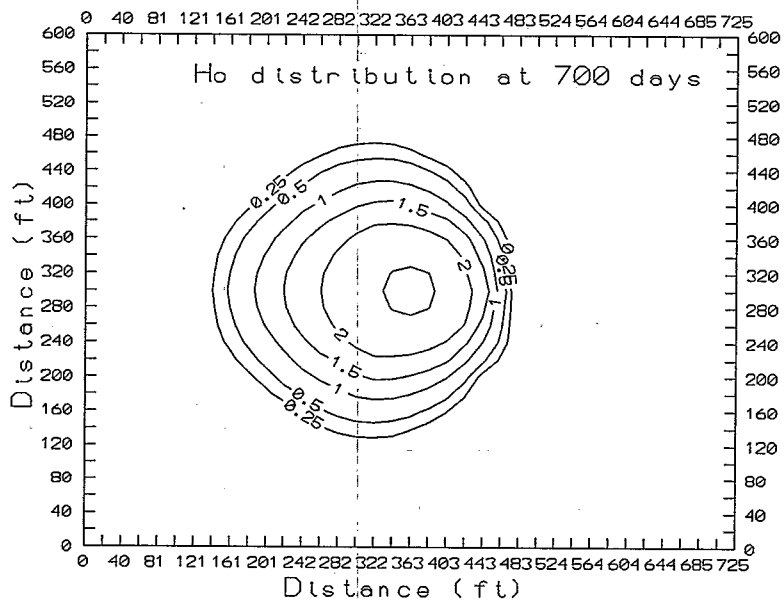
41
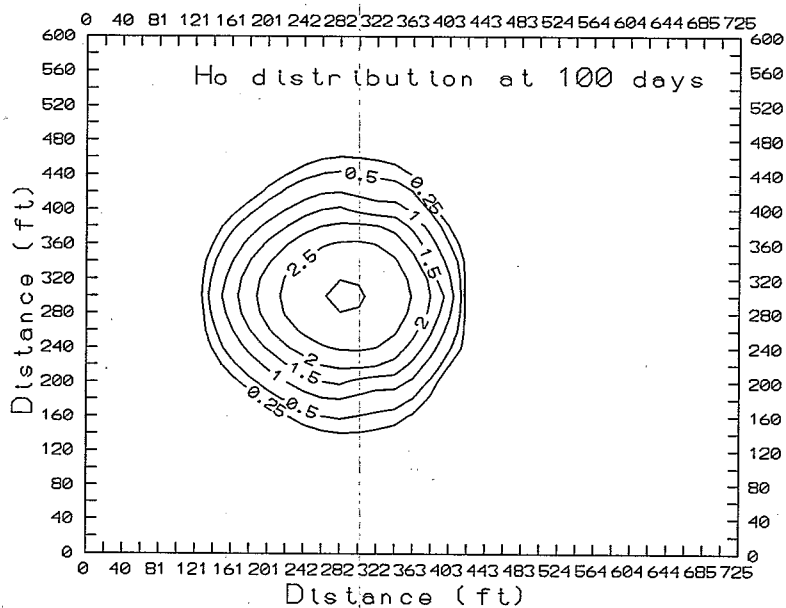
Figure 3-5. Apparent thickness 100 and 700 days after a gasoline leak predicted by ARMOS.

Section 4

Product Recovery System Design

4.1 Specification of Design Criteria

Successful remedial design for subsurface hydrocarbon spills inevitably requires compromises among a variety of technical, economical and socio-political issues. Among the factors that may be taken into consideration are:

- Control environmental and human health risks to acceptable levels,
- Meet regulatory requirements for closure,
- Minimize disruption to normal activities caused by construction/remedial measures,
- Mitigate negative publicity and potential lawsuits associated with spill, and
- Minimize total cost for site investigation and remediation.

Ideally, the first two points are consistent, but this is often not the case. In some cases, exposure risk may be low enough that no action may be warranted or free product removal in conjunction with subsequent monitoring may be an acceptable endpoint. In such cases design optimization is fairly straightforward. The objective is simply to reach asymptotic free product recovery with minimal cost, subject to constraints imposed by needs to minimize disruption, or assuage socio-political concerns. For a given design option, it is only necessary to determine if the design constraints are met and then assess the capital and operating costs amortized to present value.

Factors that will affect the cost and effectiveness of a product recovery system will include the number and location of wells and/or trenches, water and product pumping rates, treatment costs, and period of operation required to reach asymptotic product recovery. In some cases, a surrogate for cost may be employed to optimize the design. For example, if treatment costs are high, minimizing total water pumping may be an effective surrogate for design optimization. If costs associated with site disruption during remediation are high, minimizing the duration of the recovery system operation may be a reasonable surrogate for design optimization.

For most sites, regulatory requirements necessitate remediation beyond removal of free product to meet soil, groundwater or air quality criteria. In such cases, free product recovery is no longer the endpoint, but simply a first step in the remedial process. This significantly complicates the estimation of cost-effectiveness because total project cost, not simply the cost of free product recovery, must be considered. If the free product recovery design can achieve cost savings in

43

secondary remediation that exceed the additional costs of free product recovery, higher costs for free product recovery will be justified. Accurate estimation of the time and cost that will be required to reach specified soil or groundwater concentration levels is difficult. However, for a given system design, the duration of the remedial operation and the operating costs may be expected to be approximately proportionate to the mass of contaminant remaining after free product recovery is complete. Since it is generally less costly to remove a unit mass of contaminant as liquid hydrocarbon than as a dissolved or vapor phase constituent, a reasonable design criteria, in cases where soil and groundwater criteria must be met, may be to maximize the volume of free product recovered.

In summary, the most exacting method of evaluating various remedial alternatives is to perform a detailed cost analysis of all options that will meet imposed criteria (e.g., limit further plume migration, avoid construction in certain areas, meet regulatory criteria, etc.). For cases where the effort of performing such analyses is not warranted, or for preliminary screening of alternatives in any case, cost may be replaced by a surrogate variable that can be more readily evaluated.

To design a cost-effective free product recovery system, various surrogates for cost may be applicable in different circumstances. Some practical guidelines are given below.

Controlling Factor For Design	Design Surrogate
• Cleanup required to meet low soil or groundwater standards	• Maximize product recovery
• High costs associated with disruption, maintenance, monitoring or leasing	• Minimize time to asymptotic recovery
• High pumping or water treatment costs	• Minimize total water pumped

For either the full cost analysis or the cost surrogate approach, the first step is to determine whether a proposed design strategy is expected to meet pre-conditions for a valid design. Plume containment will often be specified as a prerequisite. If two pumps with a 10 gpm capacity are readily available, a prerequisite may be to limit the number of pumps and the rates to suit the equipment (if other conditions can also be met -- e.g. plume control). Site conditions may dictate other limitations, such as constraints on well placement, feasibility of constructing trenches, etc.

In order to determine if pre-conditions can be met for a given design alternative, and then to compare the optimization criteria (i.e., cost or cost surrogate), models must be used. This chapter describes methods that can be utilized to design free product recovery systems at hydrocarbon spill sites. Secondary remedial measures to reduce soil and groundwater concentrations will not be directly addressed. However, the final objectives for site closure must always be taken into account from the outset of a remedial design, beginning with the manner in

44

which recovery systems utilized for free product recovery can be optimally utilized in the final system configuration.

4.2 Effects of Well Placement and Operation

Case Study I

A numerical study of product recovery in an anisotropic fractured rock aquifer was reported by *Parker et al.* (1992). The problem involves a 27,000 gallon diesel spill investigated using the areal oil-water flow model ARMOS (*ES&T*, 1994). The distribution of the NAPL plume at the time recovery was commenced and locations of potential recovery wells are shown in Figure 4-1. Well RW-7 is about 50 feet downgradient of the spill source, wells RW-4, -5 and -6 are 250 feet downgradient, and wells RW-1, -2 and -3 are about 450 feet downgradient. The following recovery well configurations were considered in the study:

> Case A - Wells RW-1 through RW-3 operating at 0.5 gpm each,
> Case B - Wells RW-1 through RW-6 operating at 0.5 gpm each,
> Case C - Wells RW-1 through RW-7 operating at 0.5 gpm each.
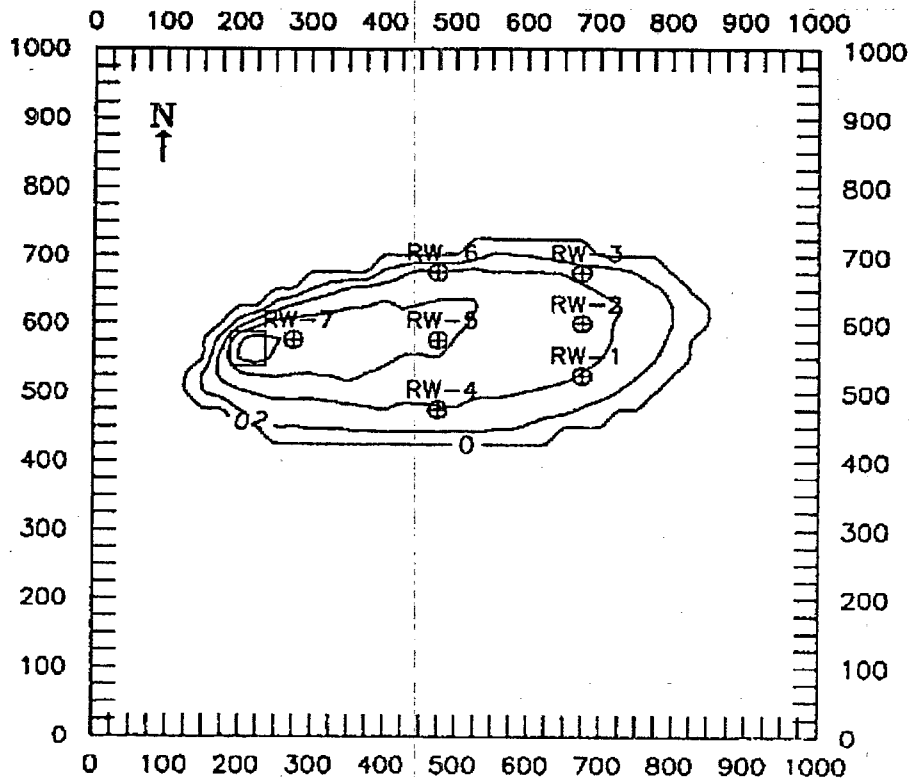

Figure 4-1. Apparent product thickness prior to recovery and well locations for Case Study.

Preliminary simulations indicated a pumping rate of 0.5 gpm yielded capture for wells RW-1, -2 and -3 when operating. Simulations of product recovery were performed for each case until asymptotic recovery was achieved. The results are summarized in Table 4-1.

Table 4-1. Summary of Recovery System Results for Case Study I.

| Case | Product Recovery | | Water Pumped (Gallons x 10⁶) | Time (days) | Oil/Water Cut x 1000 |
	Gallons	Percent			
A	5,700	21	1.94	900	2.9
B	2,900	11	1.51	350	1.9
C	2,700	10	1.01	200	2.7

The maximum recovery was obtained for the downgradient well system (Case A), which recovered 21 percent of the original spill volume. Asymptotic recovery was achieved in 900 days, after pumping 1.94 million gallons of water, giving an oil-water cut of 2.9 gallons of oil per 100 gallons water.

Adding an additional bank of wells in Case B reduced the recovery time to 350 days, and the recovery volume was cut nearly in half. The reduced recovery is a result of increased smearing in the drawdown depression associated with the additional upgradient wells. The recovery time is decreased because the average travel distance to the wells decreases. Oil-water cut dropped to only 1.9 gallons of oil per 1000 gallons of water.

Adding well RW-7 in Case C resulted in a small additional decrease in recovery volume, and reduced the recovery time to only 200 days. Oil-water cut increased to 2.7 gallons of oil per 1000 gallons of water due to the decrease in recovery time.

It is notable that increasing the number of wells decreases the volume of recovered product for this problem. This is due to the geometry of the plume and to the configuration of the recovery wells. Since the plume is rather elongated, plume capture can be achieved most efficiently with a line of wells near the toe of the plume. Additional upgradient wells do not improve containment. Increased "smearing" from the upgradient wells reduces product recovery but reduces the travel distance, thus decreasing recovery time. An option that was not investigated, but which may be advantageous, would be to include upgradient wells to reduce the travel time, but with lower pumping rates than the downgradient wells to minimize smearing.

Defining the optimal design depends on the objectives of the system. Case A provides the maximum product recovery and yields the highest efficiency, as measured by oil-water cut. It also has the lowest capital cost. Case C reaches asymptotic recovery within a much shorter time period with significantly less total water pumping. This may result in lower total operating costs, although capital costs will be greater. If residual product must be remediated, Case C becomes less attractive due to higher long term pumping needed to remove the additional mass from the soil. The results clearly illustrate the fact that recovery system design generally requires trade-offs to be made among various cost and efficiency factors.

Case Study II

An example problem is presented to investigate effects of water pumping rate, well placement and number of wells on free product recovery system effectiveness. Data for the problem was taken from a field investigation of a pipeline leak involving a mixture of gasoline, diesel and fuel oil. The estimated spill volume is 290,000 gallons. Numerical simulations were carried out using the numerical model ARMOS (*ES&T*, 1994). To simplify the analysis and to focus on the effects of design variables, effects of seasonal water table fluctuations observed in the field were not considered in the simulations.

The model domain is a 43 acre area, discretized by a mesh with 804 elements (Figure 4-2). The water table at the site occurs at a depth of 10 feet, and slightly to the west with a gradient of about 0.002. The apparent hydrocarbon thickness prior to initiation of product recovery is shown in Figure 4-2. The unconfined aquifer consists primarily of coarse sand and gravel. Soil and fluid parameters for the problem are given in Table 4-2.

Table 4-2. Soil and Fluid Parameters for Case Study II

ρ_{ro}	$K_{sw}=100$ ft d^{-1}	$S_m=0.10$
$\eta_{ro}=2.0$	$\phi=0.35$	$S_{og}=0.05$
$\beta_{ao}=3.4$	$\alpha=3.5$ ft^{-1}	$S_{or}=0.25$
$\beta_{ow}=1.42$	$n=2.0$	

Pumping wells were located as shown in Figure 4-2. RW-1 was placed downgradient of the center of the plume in order to take advantage of the natural movement of the groundwater. RW-2 was placed at the center of the plume, and RW-3 was placed near the location of the highest apparent oil thickness. Three scenarios involving different wells operating were considered:

- Case A - Pumping from well RW-1 only,
- Case B - Pumping from well RW-3 only,
- Case C ng from wells RW-1, 2 and 3.
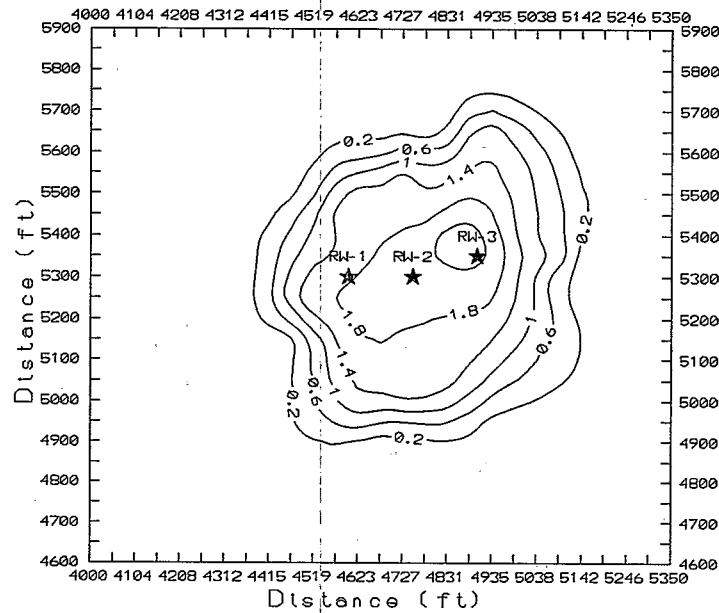
Figure 4-2. Initial well oil thickness distribution and location of recovery wells for Case Study II.

For each case, simulations were performed for several water pumping rates to determine the optimum rate for each well configuration. Water pumping rates for the different scenarios are given in Table 4-3. The rates shown for Case C are the totals for all wells, and the individual wells each were assumed to pump at one third of the total rate. Time to reach asymptotic free product recovery and the cumulative water pumping for each scenario are also summarized in Table 4-3.

48

Asymptotic product recovery versus water pumping rate for each case is shown in Figure 4-3. The results clearly indicate that for a given well configuration, an optimum pumping rate exists at which maximum product recovery is achieved. This optimum represents a trade-off between two factors. If the pumping rate is too low, the capture zone of the well field is inadequate to encompass most of the free phase plume and recovery is below optimum because plume spreading occurs. If the pumping rate is higher than necessary to achieve plume capture, recovery diminishes due to increased smearing of product within the zone of drawdown. As pumping rate increases, the final residual oil volume in the unsaturated zone increases due to smearing over the region of drawdown (Figure 4-4). However, the volume of residual in the saturated zone decreases with increasing pumping as more free product is removed and as increased smearing occurs (Figure 4-5). Maximum recovery will occur when the total residual volume (sum of saturated and unsaturated residual) is at a minimum.

Table 4-3. Pumping Rates, Times to Reach Asymptotic Recovery and Total Water Pumped for Case II Scenarios (optimum for each case in bold)

Pumping Rate	Pumping Duration			Water Pumped		
(gpm)	Case A (days)	Case B (days)	Case C (days)	Case A (M gal)	Case B (M gal)	Case C (M gal)
25	8,000	9,000	10,000	288	324	360
50	5,000	9,000	6,000	360	648	432
75	3,600	7,800	3,200	389	842	346
100	**3,000**	5,800	2,700	**432**	835	389
125	2,300	3,800	2,400	414	684	432
150	2,000	**3,300**	**2,100**	432	**713**	**454**
200	1,500	2,400	1,400	432	691	403
300	1,000	1,600	1,200	432	691	518
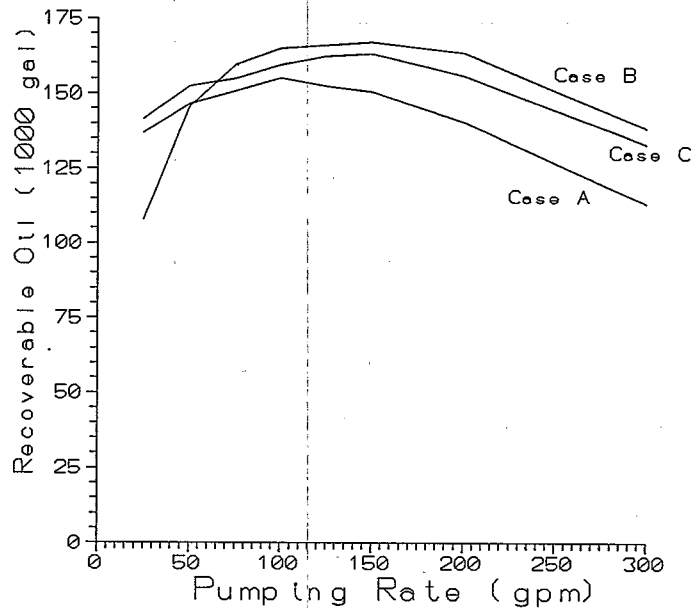
Figure 4-3. Final product recovery versus water pumping rate for Case Study II scenarios.
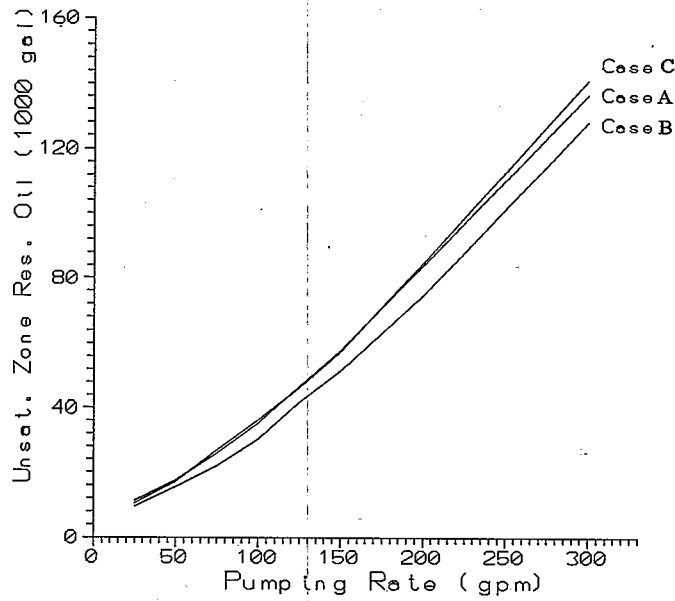
Figure 4-4. Final unsaturated zone residual product versus water pumping rate for Case Study II scenarios.

50
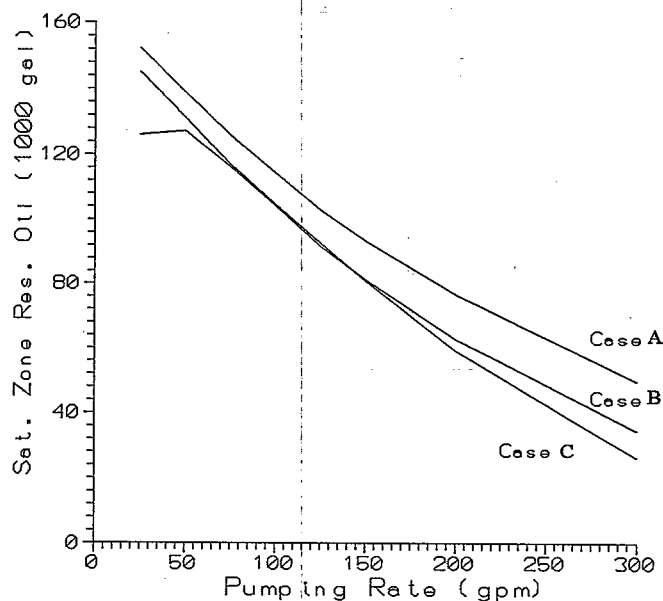
Figure 4-5. Final saturated zone residual product versus water pumping rate for Case Study II scenarios.

Case A (single downgradient well) yielded the lowest recoverable product, the lowest optimum pumping rate, and the lowest total water pumped with a recovery time of 3000 days. The downgradient location of the well allows plume perimeter control with a lower pumping rate. However, allowing the center of mass of the plume to migrate this distance evidently results in low recovery.

Case B, with a single upgradient well RW-3 operating, recovered more product than Case A or Case C at a given pumping rate and at the respective optimum pumping rates. However, the optimum pumping rate was greater for Case B than for Case A, and the recovery time was greater for Case B than for Case A or Case C. As a result, Case B required significantly greater total water pumping than the other two cases. The higher water pumping rates needed for Case B could be readily anticipated, because the upgradient position of the recovery well will require higher pumping to achieve plume capture. The higher recovery for Case B is more difficult to anticipate, since higher pumping rates would generally lead to increased smearing. Evidently, the increase in unsaturated zone residual due to higher pumping is more than offset by reduced saturated zone residual due to product recovery near the plume center that keeps the center of mass of the plume from moving downgradient. The low natural groundwater gradient is probably a significant factor resulting in the effectiveness of RW-3. Case B recovered more than Case C because the longer recovery time allowed for more residual to drain from the unsaturated zone (Figure 4-4).

51

Case C, with three wells operating, yielded somewhat less recovery than Case B but reached asymtotic recovery in the shortest time period. The total water pumping was much less than that for Case B and only slightly more than that for Case A. Although the capital cost for Case C is somewhat higher and the total recovery somewhat lower than for Case B, the system is significantly more effective in terms of total product removed, operating time, and oil pumped per volume of water operating time and operating costs.

In contrast to the results of Case Study I in the previous section, the present results indicate that upgradient wells may improve system effectiveness and even efficiency. Clearly, many factors affect the outcome of various design options and *a priori* inferences concerning system behavior are not always possible or reliable. Plume geometry, hydraulic gradient, soil and fluid properties, well placement and distribution of pumping among pumps, and many other factors must be taken into consideration. Quantitative models that can take the complex interactions of these factors into consideration are critical to making good engineering decisions.

4.3 Plume Capture and Travel Time Analysis

Evaluation of Plume Capture

As suggested in the preceding section, free phase plume control is generally a prerequisite to achieving maximum free product recovery for a given well configuration. In most cases, plume control will be a design prerequisite regardless of whether maximum recovery is the primary objective, because plume migration results in increased potential groundwater contamination and increased potential liability.

Plume containment is generally achieved by installing a system of wells and/or trenches from which water and product are pumped. For a given configuration of wells or trenches, the maximum product recovery is achieved by pumping in a manner that just controls lateral plume migration. Increasing water pumping further generally diminishes recovery. This occurs due to the increasing volume of residual product that becomes smeared over the *cone of depression* of the water table drawdown. Thus, for a given well or trench configuration, water pumping rates generally should be adjusted to just control product spreading.

In the absence of air pressure gradients, water flow occurs in response to gradients in the air-water table, Z_{aw}, often referred to as the *corrected* water table (i.e., $Z_{aw}=Z_{ow}+\rho_{ro}H_o$). For a single well, the steady state water table drawdown distribution may be computed approximately by solving the groundwater flow equation, disregarding effects of hydrocarbon on water flow. Since the saturated aquifer thickness is usually much greater than the zone with hydrocarbon, the assumption that groundwater flow is independent of the presence of hydrocarbon is usually a reasonable assumption.

The groundwater flow equations may be solved using commonly available numerical or analytical models. The simplest approach is to use an analytical solution for steady state flow to a point source or sink (i.e., an injection or pumping well), and to superpose the resulting drawdown

to approximate a system of wells or a line sink (i.e., a trench). Superposition is strictly valid for confined aquifers, but may be used to approximate unconfined flow if drawdown is small compared to the aquifer thickness. From the principle of superposition, the effect of multiple wells on the water table distribution (assuming no air pressure gradients) is computed by

(4.1)

$$Z_{aw} = Z_{aw}^{O} - \sum_{j=1}^{J} \Delta Z_{aw_j}$$

where Z_{aw}^{O} is the air-water table elevation at a given location without pumping, ΔZ_{aw}, is the drawdown at the location attributable to well j, and J is the total number of wells. The pre-pumping water table configuration, $Z_{aw}^{O}(x,y)$, may be determined by kriging air-water table elevations at monitoring wells onto a grid and the post-pumping water table may be computed from (4.1) and drawdowns at grid points attributable to each well.

Horizontal flow of separate phase hydrocarbon occurs in response to gradients in the air-oil table elevation, Z_{ao}, in the absence of air pressure gradients. Once we determine the air-water table, the air-oil table may be estimated for each point in the computational grid as

(4.2)

$$Z_{ao} = Z_{aw} + (1 - \rho_{ro})H_o$$

where Z_{aw} is the post-pumping water table, ρ_{ro} is the oil specific gravity, and H_o is the apparent product thickness at the location prior to commencing pumping interpolated from monitoring well data. Equation (4.2) yields an approximation of the air-oil table after water flow approaches steady state conditions, but before significant oil redistribution has occurred. Since oil tends to accumulate at the wells and gradually diminishes in thickness near the plume perimeter, the oil gradient around the edge of the plume, computed from (4.2), will generally be an upper estimate. Thus, if we can show that the gradient of Z_{ao} is flat or towards the recovery wells at all locations around the plume perimeter, control of plume migration should be achieved for the assumed pumping conditions.

To evaluate whether or not oil plume control will be achieved, we first delineate the plume perimeter by a small apparent product thickness contour (for example, 0.1 ft). Inspection of the direction of the air-oil gradient on the plume perimeter indicates whether plume control has been achieved. Alternatively, oil streamlines perpendicular to Z_{ao} contours may be drawn to assess capture by the recovery well system.

Estimation of Recovery Time
Once flow rates have been determined for a given well or trench configuration that achieves free phase plume control, an estimate of the time to reach asymptotic recovery may be made. An approximate method for doing this is based on the travel time analysis discussed in Section 3.3.

53

The first step is to draw streamlines perpendicular to the estimated steady state Z_{ao} contours. The longest travel path between a recovery well or trench and the perimeter of the plume should be identified, as this will control the time required to reach asymptotic free product recovery. The travel path may be divided into a number of intervals. The air-oil gradient for an interval times the mobility coefficient (Section 3.3) gives the travel time for the interval. Summing the interval travel times will yield the total travel time.

Example Problem - Section 3.3 showed that the mobility factor M_o can be multiplied by the water table gradient to estimate the average oil velocity (v_o) during redistribution without pumping. The same principle can be applied to the case of oil moving to a well or trench, with the added complication that the pathline may not be straight nor the gradient constant. In these situations, the pathline can be broken into smaller segments that are approximately straight with uniform gradient.

Returning to the example of Section 4.2, we analyze travel time using the optimum case of three recovery wells (Case C) pumping at a combined rate of 150 gpm. Figure 20 shows the initial distribution of the free phase plume overlain with pathlines. Each pathline depicts the movement of an oil "particle" from the edge of the plume to a well. The travel time along each pathline is computed using the steady state water flow field. The average velocity of the oil phase can be computed from the mobility factor M_o and the gradient in Z_{ao}, via eq. (3.11). During oil recovery, Z_{ao} will drop continuously until it reaches the water table. Thus, for a steady state approximation, we may use the water table drawdown around a recovery well as an estimate of Z_{ao}.

54
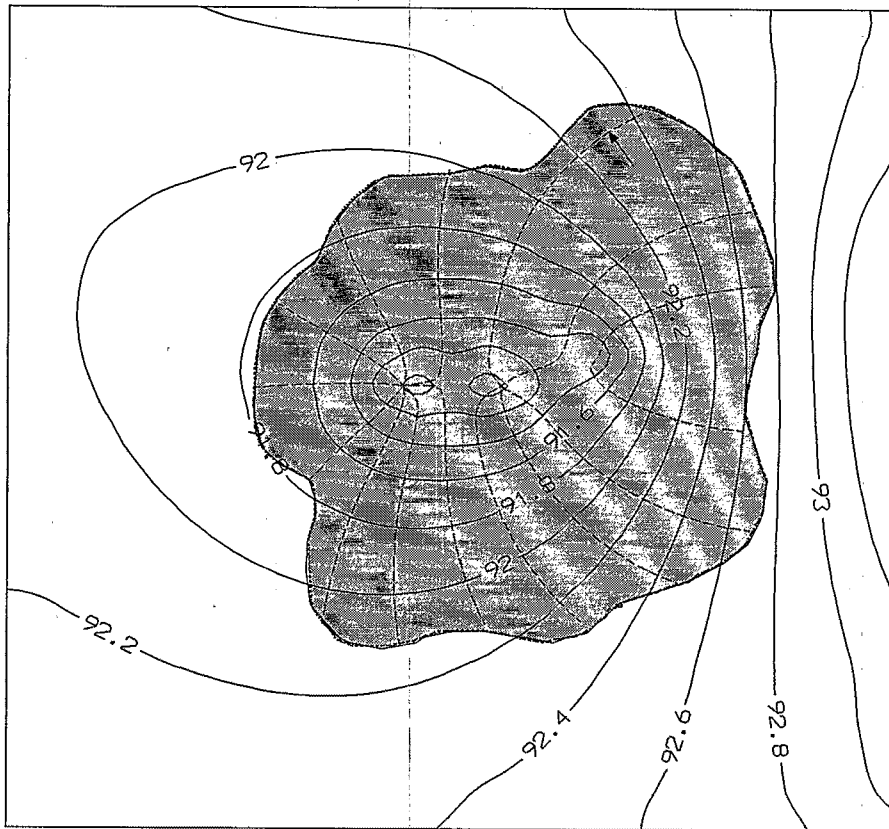
Figure 4-6. **Flow net for travel time analysis. Solid lines are steady state Z_{aw} contours, dashed lines are streamlines, area within dark line is plume, arrow shows longest path.**

The longest pathline in Figure 4-6 depicts the maximum travel distance for oil during free product recovery. Thus the travel time along this pathline should correspond to the time needed to reach asymptotic recovery. For the longest pathline, an oil travel time of 2360 days from the edge of the plume to the well is predicted using the maximum mobility factor M_o^{max} (eq. 3.12). This is slightly higher than the recovery time predicted by the transient oil-water flow model ARMOS of 2100 days (Table 4-3).

4.4 Estimation of Recoverable Product

Description of Method

Methods for estimating the volume of *free oil* were discussed in Section 3.2. Unfortunately, only a fraction of this volume will be recoverable as a separate phase, due to various processes that lead to the occurrence of *residual oil*. We distinguish between residual oil in the liquid-saturated zone, which occurs as hydraulically discontinuous blobs trapped within a continuous water phase, and residual oil in the unsaturated zone, which occurs as thin films and as pendular rings of oil at particle contacts. The *recoverable volume* is given by

$$\sum_{\infty} = \sum_{of} - \sum_{ot} - \sum_{og} \qquad (4.3)$$

where $\sum_{of}$ is the current free oil volume computed as described in Section 3.2, $\sum_{ot}$ is the volume of current free oil that becomes trapped in the liquid saturated zone, and $\sum_{og}$ is the volume of current free oil that is retained as residual oil in the unsaturated zone.

The total saturated and unsaturated zone residual oil volumes may be computed from specific volumes on a grid as

$$\sum_{ot} = A \sum_{i=1}^{N} V_{ot_i} \qquad (4.4)$$

$$\sum_{og} = A \sum_{i=1}^{N} V_{og_i} \qquad (4.5)$$

where V_{ot_i} is the residual oil specific volume that is trapped in the liquid saturated zone at location i, V_{og_i} is the residual oil specific volume held against gravitational drainage in the unsaturated zone, and A is the element area.

Residual oil in the unsaturated zone arises during periods of falling Z_{ao}, when downward oil redistribution eventually becomes negligible under gravitational forces, as oil saturation reaches a critical value referred to as the *unsaturated zone residual saturation* (see Section 2.4). The increase in residual oil specific volume in the unsaturated zone due to a drop in the air-oil table, ΔZ_{ao}, is described by equation (2.12) which is applied in a series of pseudo "time-steps" until the cumulative change in Z_{ao} is equal to $\Delta Z_{aw} + (1 - \rho_{ro})H_o + \Delta Z_R$ where ΔZ_{aw} is the water table drawdown, H_o is the initial well oil thickness at the location, and ΔZ_R is the regional change in Z_{ao} associated with seasonal water table fluctuations.

Saturated zone residual oil specific volume may be computed as described in Section 2.4 for the anticipated change in the oil-water table elevation ΔZ_{ow}. With removal of product from

the formation during steady water pumping, the oil-water table will increase until well oil thickness (H_o) approaches zero at which point $Z_{ow}=Z_{aw}$. Also considering possible water table fluctuations, $\Delta Z_{ow}=\rho_{ro}H_o+\Delta Z_R$, where ΔZ_{ow} is the cumulative change in Z_{ow}, ΔZ_R is the regional change in Z_{ow} due to seasonal water table fluctuations, and H_o is the initial well product thickness. The latter is corrected for residual oil in the unsaturated zone by computing the value of H_o at each grid point corresponding to the initial V_{of} minus $2 \times V_{og}$, where the factor 2 takes into consideration the fact that gradual oil drainage from the unsaturated zone reduces saturated zone trapped oil. A correction for the change in capillary fringe thickness due to hysteresis may be applied to ΔZ_{ow} as described in Section 2.4.

The estimates of asymptotic recoverable product volumes described above are based on projected estimates of residual oil in the saturated and unsaturated zones, associated with changes in fluid table elevations due to water pumping and product removal. This assumes that lateral plume spreading is controlled. If this condition is not met, the actual recoverable product may be substantially less than the computed values, since residual volumes will increase as the plume spreads over a greater area. **Therefore, it is very important to verify plume control by determining that oil gradients are inwards on the plume perimeter, before performing recoverable product calculations.**

Example Problem - The following example demonstrates the calculation of residual and recoverable oil specific volumes. To compute total recovery, similar calculations must be repeated for each location where fluid levels are known or interpolated, so that actual volumes can be computed by summation over the area. The example problem continues with the problem introduced in Section 3.2, which has an initial apparent product thickness of 3 feet, with the air-oil table at 93 feet and the oil-water table at 90 feet. Pumping is assumed to cause a 1.5 foot drawdown in Z_{ao} at the location. Soil and fluid properties for the problem are given in Table 5. A step-by-step description of the methodology for computing residual and recoverable product specific volumes is given below for the example problem.

1. The initial free oil specific volume prior to beginning pumping is computed as described in Section 3.2., which indicates $V_{of}=0.309$ feet.

2. The average initial free oil saturation is estimated as

$$\overline{S}_{of}=\frac{V_{of}}{\phi H_o}$$

which gives a value of 0.294.

3. An initial estimate of the unsaturated zone residual oil specific volume, V_g^{init}, is computed as

$$V_g^{init}=Min(V_{g1},V_{g2},V_{g3})$$

57

where

$$V_{g1} = \phi S_{og} \Delta Z_{aw} = 0.0315 \text{ feet}$$

$$V_{g2} = \phi \overline{S}_{of} \Delta Z_{aw} = 0.1544 \text{ feet}$$

$$V_{g3} = V_{of}^{init} \left[1 - \exp\left(\frac{\Delta Z_{aw}}{H_o}\right) \right] = 0.1217 \text{ feet}$$

which gives $V_g^{init} = 0.0315$ feet.

4. A revised estimate of the free oil specific volume corrected for oil retention in the unsaturated zone is computed as

$$V_{of}^{new} = V_{of}^{init} - 2V_g^{init}$$

where the factor 2 is assumed to account for the finite time for oil to drain to a new vertical equilibrium after the onset of pumping, during which time product recovery will proceed. The corrected free oil specific volume for the example is $V_{of}^{new} = 0.246$ feet.

5. A revised value of apparent product thickness corresponding to the updated free oil specific volume of 0.246 feet is determined by interpolation from a table of H_o versus V_{of} generated using the method described in Section 3.2, yielding $H_o^{new} = 2.65$ feet.

6. To simulate oil recovery H_o is reduced to zero in N "time- steps", causing Z_{ao} to drop and Z_{ow} to rise in incremental steps. The incremental changes in Z_{ao} and Z_{ow} are calculated as

$$\Delta Z_{ow} = \frac{\rho_{ro} H_o - Z_c}{N}$$

$$\Delta Z_{ao} = \frac{H_o (1 - \rho_{ro})}{N}$$

where Z_c is the change in the capillary fringe due to reversal from oil imbibition to oil drainage given by (2.11e). For the example problem, $Z_c = 0.67$ feet and employing $N = 30$ "time-steps" gives $\Delta Z_{ao} = 0.0177$ feet and $\Delta Z_{ow} = 0.0484$ feet. Calculations of residual oil in the saturated and unsaturated zones for 30 "time-steps" are shown in spreadsheet form in Table 4-4 with columns in the spreadsheet computed as follows:

Table 4-4. Spreadsheet for Calculation of Residual and Recoverable Oil Specific Volume

A	B	C	D	E	F
Step	H_o (feet)	V_{of} (feet)	S_{of} (feet)	S_{ot} (feet)	S_{og} (feet)
0	2.65	0.2462			
1	2.56	0.2307	0.263	0.200	0.060
2	2.47	0.2156	0.255	0.200	0.060
3	2.39	0.2006	0.247	0.200	0.060
4	2.30	0.1861	0.238	0.200	0.060
5	2.21	0.1720	0.229	0.200	0.060
6	2.12	0.1582	0.220	0.200	0.060
7	2.03	0.1449	0.211	0.200	0.060
8	1.94	0.1320	0.201	0.200	0.060
9	1.85	0.1194	0.192	0.192	0.060
10	1.77	0.1074	0.182	0.182	0.060
11	1.68	0.0960	0.171	0.171	0.060
12	1.59	0.0850	0.161	0.161	0.060
13	1.50	0.0746	0.150	0.150	0.060
14	1.41	0.0648	0.140	0.140	0.060
15	1.32	0.0556	0.129	0.129	0.060
16	1.24	0.0471	0.118	0.118	0.060
17	1.15	0.0393	0.107	0.107	0.060
18	1.06	0.0321	0.096	0.096	0.060
19	0.97	0.0257	0.085	0.085	0.060
20	0.88	0.0200	0.074	0.074	0.060
21	0.79	0.0151	0.063	0.063	0.060
22	0.71	0.0110	0.053	0.053	0.053
23	0.62	0.00759	0.043	0.043	0.043
24	0.53	0.00492	0.034	0.034	0.034
25	0.44	0.00292	0.025	0.025	0.025
26	0.35	0.00153	0.018	0.018	0.018
27	0.26	0.00066	0.012	0.012	0.012
28	0.18	0.00020	0.006	0.006	0.006
29	0.09	0.00003	0.003	0.003	0.003
30	0.00	0.00000	0.001	0.001	0.001
				3.4373	1.453

Column A: This column is simply an integer step number, 1, 2, N.

Column B: The value $H_{o_+}^{new}$ is input in row 1. At each new step, $H_o/30$ is subtracted from the previous H_o to reduce H_o to zero in 30 steps.

Column C: V_{of} is computed from the corresponding H_o in column A using the method described in Section 3.2.

Column D: The average free oil saturation is calculated as $\overline{S}_{of} = \dfrac{V_{of}}{\phi H_o}$.

Column E: The residual oil saturation in the saturated zone for the step is computed as

$$S_{ot} = Min\ (S_{or}, \overline{S}_{of})$$

This column is summed to obtain $\Sigma S_{ot}=3.473$ which is multiplied by $\phi \Delta Z_{ow}=0.0169$ to yield $V_t=0.0587$ feet.

Column F: The residual oil saturation in the unsaturated zone for the step is computed as

$$S_{og} = Min(S_{og}, \overline{S}_{of})$$

This column is summed to obtain $\Sigma S_{ot}=1.453$ which is multiplied by $\phi \Delta Z_{ao}=0.0062$ to yield $V_g=0.009$ feet. This value is added to V_g^{init} from Step 3 above to obtain $V_g^{total}=0.0405$ feet.

$$V_{rec}=V_{of}^{init}-V_g^{total}-V_{ot}=0.21$$

Finally, recoverable oil specific volume can be calculated as

In this example, more than half the oil has been recovered because the initial apparent oil thickness (H_o) was a relatively large value of 3 ft. If this problem were repeated using an initial H_o of 1 ft, then only 17 percent of the oil would be recovered. Thus, a large percentage of the oil may be recovered from the center of a plume where H_o is large, but most of the oil around the edges of the plume will be trapped as residual.

Verification of Recoverable Oil Algorithm

The residual and recoverable oil calculations described above, as implemented in the program SPILLCAD (ES&T, 1994) which also performs areal interpolation and integration of specific volumes, were verified by comparison with a model for transient oil and water flow. The test problem is the gasoline spill described in Section 3.3 with pumping from a single recovery well placed down-gradient of the center of the plume initiated 100 days after the leak stopped.

Water is pumped from the recovery well at rates varying from 0 to 18 gpm, while oil is recovered at a rate to maintain product thickness in the well near zero. Transient oil and water pumping was simulated using the numerical model ARMOS (ES&T, 1994). Both models predicted plume containment at a pumping rate of about 4 gpm. Comparisons of recoverable oil, unsaturated zone residual oil, and saturated zone residual oil as functions of water pumping rate predicted by the two models are shown in Figures 4-7, 4-8, and 4-9.

SPILLCAD results for pumping rates less than 4 gpm are shown as dashed lines because residual and recoverable estimates using this approach are not meaningful unless containment is achieved. The pseudo-transient calculations in SPILLCAD somewhat under-predict product recovery, mostly because it traps more oil than the more rigorous numerical model in the saturated zone. This effect can be explained by movement of oil to the well as drawdown occurs. In the early stage of recovery, a certain amount of oil will be recovered before water flow reaches steady state.

During this period, Z_{ow} drops with Z_{aw}, even though oil is being recovered. SPILLCAD cannot capture this transient effect, as the pseudo time-steps always cause Z_{ow} to rise and trap oil (see previous example problem). Considering this limitation, the agreement between the two models is quite good. In both models, residual oil in the unsaturated zone increases with pumping rate as oil smears over a larger volume of soil. This causes residual oil in the saturated zone to decrease with pumping rate as less free oil redistributes below the water table.
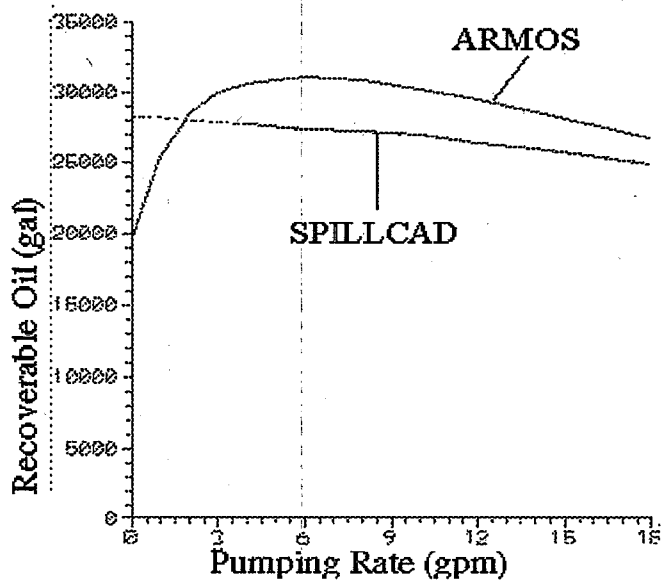
61

Figure 4-7. Comparison of recoverable oil volume versus water pumping rate for ARMOS and SPILLCAD. Dashed line indicates pumping rate too low to provide plume capture.
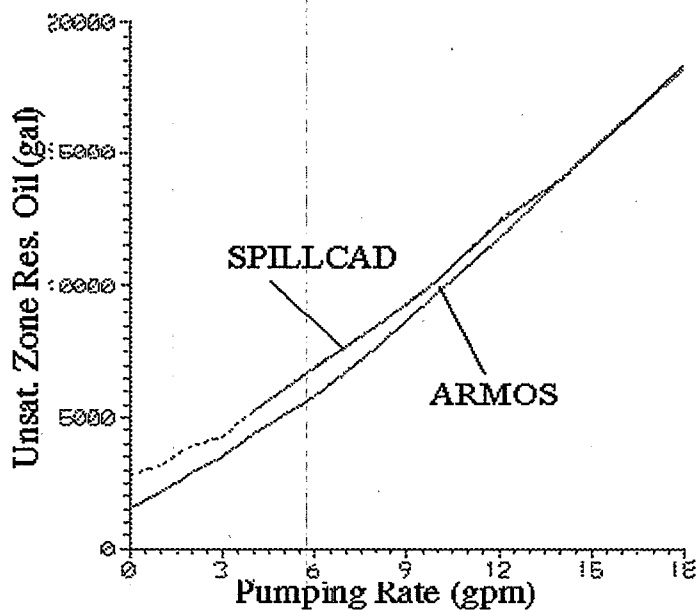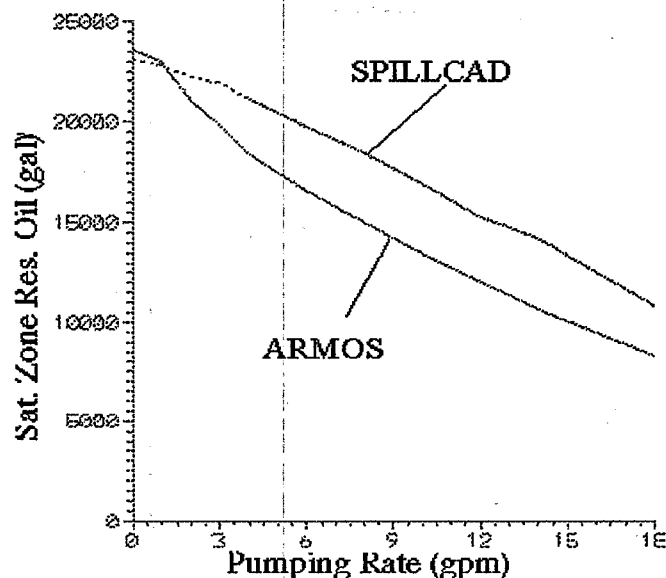

Figure 4-8. Comparison of unsaturated zone residual oil volume versus water pumping rate for ARMOS and SPILLCAD. Dashed line indicates pumping rate too low to provide plume capture.

Figure 4-9. Comparison of saturated zone residual oil volume versus pumping rate for ARMOS and SPILLCAD. Dashse line indicates pumping rate too low to provide plume capture.

4.5 Considerations in Using Trenches

Trenches have a number of advantages over recovery wells in circumstances where they are practical to install. The main limitations of using trenches are:

- Depth to free product pool makes trench construction impractical or too costly, or

- Buildings, pipelines, utilities or other features prevent trench construction.

When these factors do not preclude the applicability of a trench, another factor that must be given consideration is the head drop that occurs along the length of the proposed trench. If the trench crosses the natural water contours, the natural flow will be altered even if no water is pumped. Because the resistance to flow in a trench is usually much less than that in soil, the head difference along the length of a trench will be small, and water will recharge on some sections of the trench and discharge on others. This may have an undesired effect on the groundwater flow and on the plume. Numerical models may be used to assess the effects. If the trench placement cannot be altered to avoid cutting across the water contours, consideration should be given to constructing the trench in segments, which may be staggered and controlled at different elevations.

63

A major advantage of using trenches for free product plume control is that definitive plume containment can be achieved with little or even no water pumping. If the trench intercepts the oil plume pathline, skimming product from the trench without water pumping will prevent further free phase plume migration past the trench. Even if product thickness in the trench is nonzero due to placement or operating conditions for skimming pumps, positive plume containment can be achieved due to a *capillary barrier effect* which prevents oil infiltration through the downgradient trench wall. As indicated by the Laplace capillary equations (eq. 2.2), a finite nonwetting phase pressure (hence, trench oil thickness) is needed before nonwetting fluid (oil) can displace a wetting phase (water). The phenomenon is evident in the form of the relationship between free oil specific volume or oil transmissivity and apparent oil thickness discussed in Section 2.5. This finite oil thickness, which is greater for finer soils, is required for oil entry into the soil. This thickness may range from a few inches in a sandy soil to several feet in a fine grained soil. The capillary barrier effect provides a safety factor for free phase plume control using trenches.

As a product recovery measure, trenches are generally both more efficient and more effective than a line of wells. Because the flow field to a well is radially converging, while flow to a trench is planar, a larger drawdown will be needed for wells to obtain the same oil recovery rate achieved by a trench. Furthermore, because residual oil will be increased by the greater drawdown, the ultimate product recovery will typically be lower for the well system.

The recovery rate for free product in a trench may be estimated directly from Darcy's law as

$$R_o = T_o L \frac{dZ_{ao}}{dx}$$

(4.6)

where R_o is the oil recovery rate (e.g., cubic feet per day), T_o is the oil transmissivity at the trench (see Section 2.5), L is the trench length, and dZ_{ao}/dx is the air-oil table gradient at the trench wall (assuming no air pressure gradient). For a given trench configuration and water pumping rate (hence air-water table), the maximum oil recovery rate will be achieved by maintaining the oil thickness in the trench near zero, although oil recovery rate will be relatively insensitive to the oil thickness in the trench. This is because the product thickness in the soil adjacent to the trench will adjust naturally to form an oil seepage face with an upper elevation that maximizes the oil flow rate into the trench. The maximum flow rate corresponds to the maximum of the product of oil transmissivity, which increases with oil thickness and hence oil seepage face elevation, and decreases with oil gradient, which decreases with increasing oil seepage face elevation. Unless the oil level in the trench is raised above the natural seepage face elevation, negligible reduction in flow rate will be observed. Similar seepage face phenomena are observed in wells.

4.6 Vacuum Enhanced Free Product Recovery

Basic Concepts

Vacuum enhanced recovery (VER) is a modification of conventional free product recovery system design, in which a vacuum is applied to the well bore to increase the hydraulic gradient. In conventional product recovery systems, free phase hydrocarbon is removed by pumping hydrocarbon from recovery wells, usually in conjunction with water pumping to increase the gradient and the radius of influence. The efficiency of such systems depends on soil and fluid properties, environmental variables, as well as design variables such as the number of wells and the rates of water pumping. Since light hydrocarbons float on the water table, the radius of influence for hydrocarbon flow is directly related to the cone of depression produced by pumping groundwater. When the pumping rate is too low, hydraulic control of the free product plume is not achieved and spreading of the plume leads to an increase in residual product. Increasing the water pumping rate generally increases the rate of product recovery initially and may increase the total recovery up to the point where plume control is achieved. However, for large drawdowns associated with high pumping rates, the mobile hydrocarbon is smeared at residual saturation in the unsaturated zone. Therefore, an optimal pumping rate exists for maximum product recovery for a given well configuration at which the pumping rate is high enough to yield plume capture.

Applying a vacuum to a recovery well enables the piezometric gradient for oil and water flow to a well to be increased, without a corresponding reduction in the air-oil and oil-water tables. When a vacuum is applied in a well, liquids in the well and the soil will rise due to the reduced pressure above the fluid interfaces. This phenomenon called upwelling can be reversed by lowering the water pressure in the bore hole and increasing the water pumping rate. The locations of the piezometric surfaces near a recovery well before and after the vacuum is applied are shown in Figure 4-10. The application of vacuum (h_a) lowers both the oil and the water piezometric surfaces (Ψ_o and Ψ_w), which results in an increased gradient for flow. If the oil and water pump intake (or control switch) elevations are not altered, increased water and oil flow rates may be achieved without lowering the liquid levels and thus without increasing the amount of residual product in the unsaturated smear zone. The radius of influence of the air vacuum will depend to a significant degree on the magnitude of vertical "leakage" of air that occurs from the ground surface to vacuum wells.
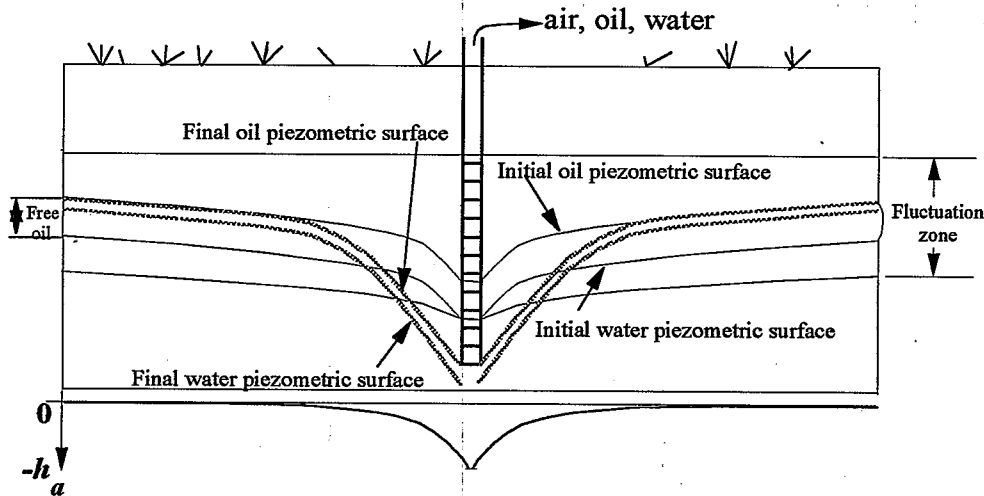
Figure 4-10. Schematic of vacuum enhanced product recovery system.

Example Problem Description - An example problem is presented to investigate the effects of various soil and design variables on VER system effectiveness. The problem is the same as Case Study II discussed in Section 4.2 involving a pipeline leak of gasoline, diesel and fuel oil with three recovery wells (Case C). ARMOS was used to simulate water, NAPL and air flow. Water and NAPL recovery was simulated assuming water pumping was performed at a specified rate, while NAPL was removed at a rate sufficient to maintain zero well product thickness. Air flow was controlled by specifying the air vacuum at the well, assumed to be 3.5 feet of water head. The ground surface was assumed to be either covered or uncovered. For the covered case, no air leakage from the ground surface was permitted, while vertical flow from the ground surface was considered for the uncovered case. The following three cases were considered:

1. Base case involving conventional product recovery without vacuum,
2. VER system without a surface cover, and
3. VER system with a surface cover.

For each of these cases, several simulations were performed with fluid levels specified at different drawdowns relative to the initial water table elevation. Water pumping rates varied from 13 to 103 gpm for the various subcases. For the assumed vacuum and well placement, the optimum drawdown (or water pumping rate) to maximize product recovery may be determined.

A comparison of the predicted cumulative product recovery versus time for the three cases at a water pumping rate of 52 gpm, which is close to the optimum rate for maximum recovery for all cases, is shown in Figure 4-11. The results indicate that the recovery rate for the VER system with a covered surface is initially nearly 70 percent greater than the conventional recovery system (no VER). However, the difference in recovery rates narrows over time, such that the VER system yields only about 7 percent more cumulative recovery after 3000 days of operation. The VER system with an uncovered ground surface exhibits a recovery curve that is about half way

66

between the covered VER system and the no VER system.

The differences between the VER systems with and without a cover are due to the effects of vertical air leakage on the radius of influence of the vacuum wells. As seen in Figures 4-12 and 4-13, the radius of influence of the vacuum wells (operationally defined as a vacuum of 0.01 feet of water) is much smaller for the uncovered than for the covered case. Due to the limited areal extent of the vacuum, effects on hydrocarbon recovery are greatly reduced. It is important to note that the "covered" case assumed that the ground surface is perfectly sealed to air flow. Pavements and buildings seldom closely approximate such an ideal condition, and vertical leakage must always be considered a real possibility.
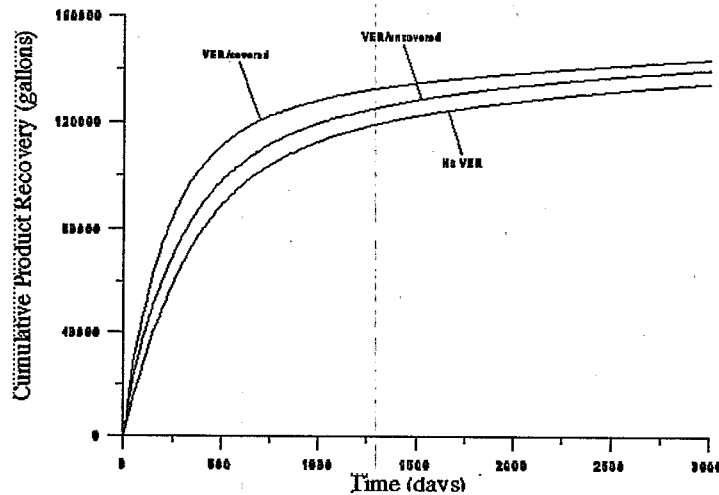
Figure 4-11. Effects of VER on product recovery for systems at a water pumping rate near optimum for recovery.

Vacuum Zone
of Influence

Extent of Free
Product Plume

Water Piezometric
Surface
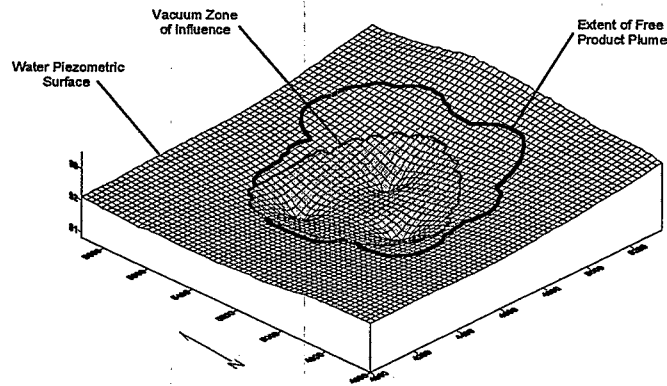
Figure 4-12. Zones of influence for water and air phases in VER system with cover.

Vacuum Zone
of Influence

Extent of Free
Product Plume

Water Piezometric
Surface

Figure 4-13. Zones of influence for water and air phases in VER system without cover.

Figure 4-14. Asymptotic product recovery versus liquid drawdown with and without VER.

Discussions of conventional product recovery system design in Section 4.2 indicated that an optimum water pumping rate will exist that yields the maximum asymptotic product r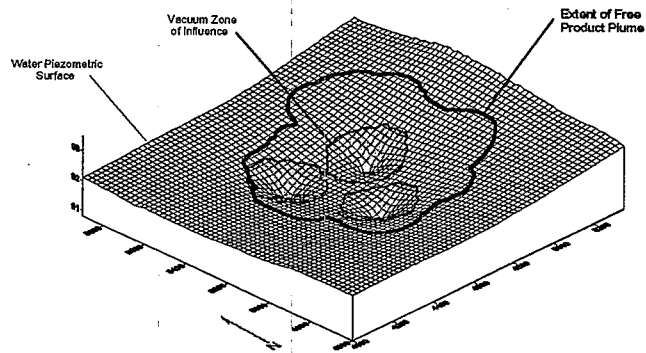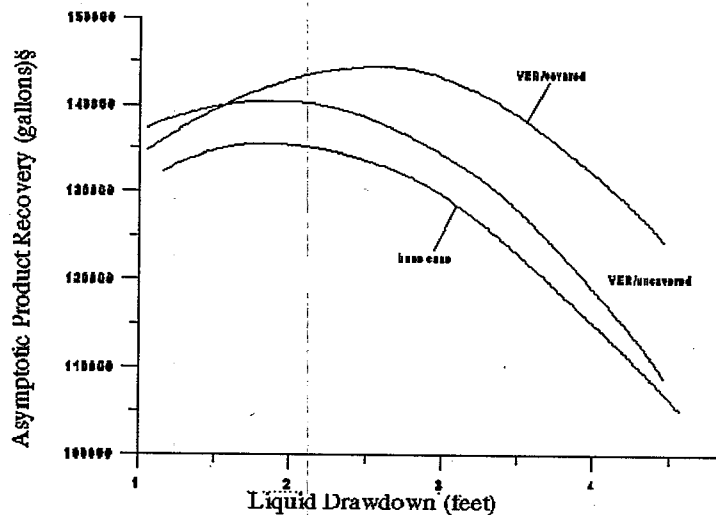ecovery for a given well configuration. To determine how vacuum affects recovery optimization, we turn to results of simulations of product recovery for varying piezometric drawdown. Piezometric drawdown is the difference between the initial static water level and the well piezometric head ($\Psi_w = Z_{aw} + h_a$). Asymptotic product recovery versus drawdown for all three cases indicate an optimum piezometric drawdown of about 2.0 feet for the no vacuum and uncovered VER cases and about 2.5 feet for the covered VER case (Figure 4-14). These correspond to pumping rates of about 50 and 60 gpm, respectively.

Evidently, the vacuum area of influence for the uncovered case is so small that the optimum recovery is controlled by the water pumping needed to control the plume perimeter, which is beyond the influence of vacuum wells. For the covered case, the vacuum exerts some influence near the plume perimeter and a small increase in pumping is needed to overcome the mounding effect. It is interesting that the optimum scenarios for the uncovered and covered cases correspond to well bore liquid levels that are about 1.0 and 1.5 feet *above* the initial static levels.

Additional simulations were performed with different vacuums applied to the wells. The results indicate that higher vacuum increases the initial rate of hydrocarbon recovery substantially, but results in only small increases in final recovery. The results indicate that vacuum enhanced product recovery may enable slightly higher asymptotic recovery to be achieved. However, the primary utility of VER is to increase the recovery rate and hence reduce the time to complete free product recovery. The extent to which this objective can be achieved will depend on the area of influence for the vacuum that can be achieved, which will in turn depend strongly on the extent of

69

vertical air leakage that occurs.

Some general conclusions concerning VER follow:

- For specified water and oil pump levels in recovery wells, water and oil recovery rates will increase as the vacuum is increased,

- To achieve maximum product recovery, well placement and water levels in wells must be maintained at a level that will yield plume containment,

- If the vacuum area of influence is smaller than the oil capture area, vacuum will have a minor effect on the asymptotic recovery or on the optimal pumping rate at which this occurs,

- The effectiveness of VER decreases as the vacuum area of influence decreases, which occurs as vertical air leakage increases and air flow rate decreases.

Effects of VER on residual soil concentrations in the unsaturated zone, due to extraction of volatile components and to enhanced biodecay associated with increased oxygen fluxes, have not been considered in the above discussion. In practice, these factors will provide additional benefits of VER systems. If a soil vapor extraction or bioventing system is under consideration for treatment of residual contamination, and hardware requirements are compatible with the operation of a VER system, consideration should be given to co-design of the vapor extraction/bioventing system to function initially as a VER system to maximize efficiency and reduce overall system cost.

Section 5

Case Study of Spill Site

5.1 Introduction

This case study presents an application of the methodology discussed in this report for assessment and remedial design of a hydrocarbon spill site. The study is based on a release documented by *Dakin et al.* (1992), which occurred in British Columbia. The study was conducted to illustrate how modeling can be employed to provide information to facilitate decision-making when characterization data is limited and time is a significant constraint. Specifically, modeling was performed (1) to assess the contamination at the site, and (2) to design a recovery system to remediate the phase separated hydrocarbon lens existing at the water table.

The spill of concern involved the accidental release of xylene from an elevated platform into underlying soils (see Figure 5-1). Xylene infiltrated the soils and ponded on the water table. Response activities were constrained at the site due to existing structures and railroad operations. In particular, the property owner required unlimited access to the site along the adjacent rail lines. Given these constraints, modeling was considered an essential tool in the assessment and remedial operations.

5.2 Model Application for Site Assessment

Site characterization activities performed shortly after the release determined the approximate extent of contaminated soil, contaminated groundwater, and a separate phase lens of xylene (Figure 5-2). The contamination occurred in fill material consisting of medium to fine sand. The fill overlies natural sediments composed of low permeability silts. At the time of the release, the water table was located approximately 4.5 feet below the ground surface. In the area of the spill, the water table slopes to the south and west with a gradient of approximately 0.02 upgradient of the spill but flattens to a gradient of 0.005 downgradient of the release (Figure 5-3). Regional hydrologic information suggested that the water table fluctuates between 0.75 to 1.5 feet annually due to seasonal variations in precipitation and evaporation.
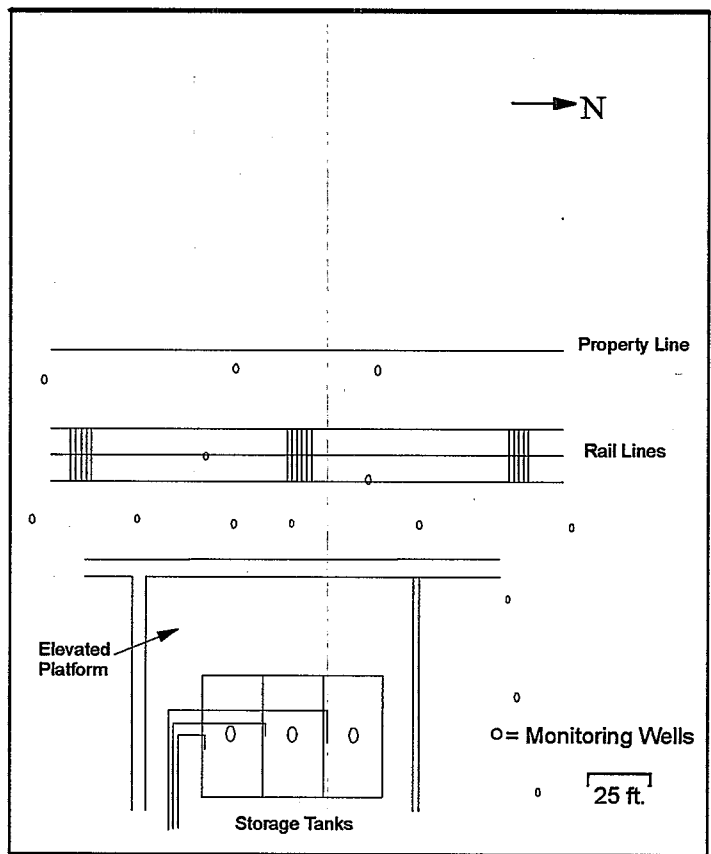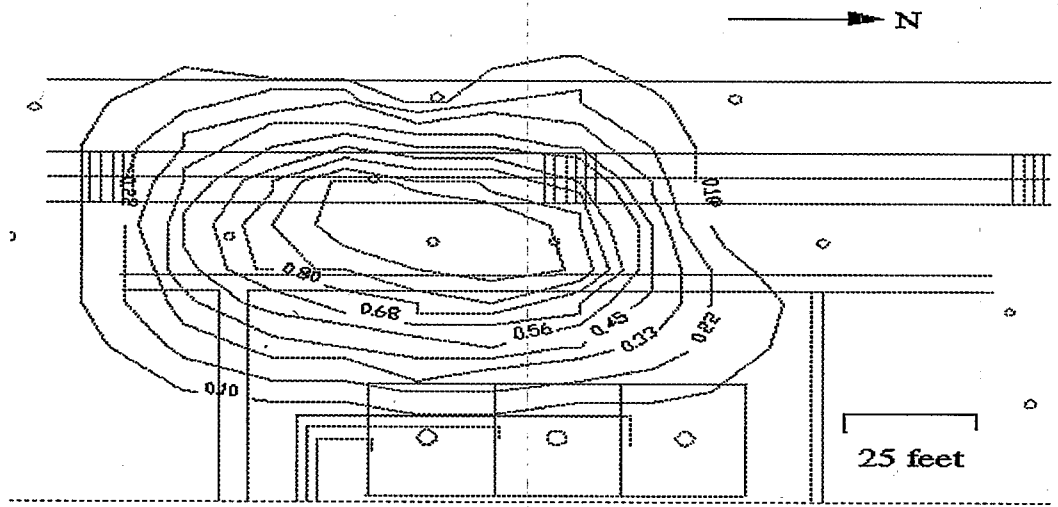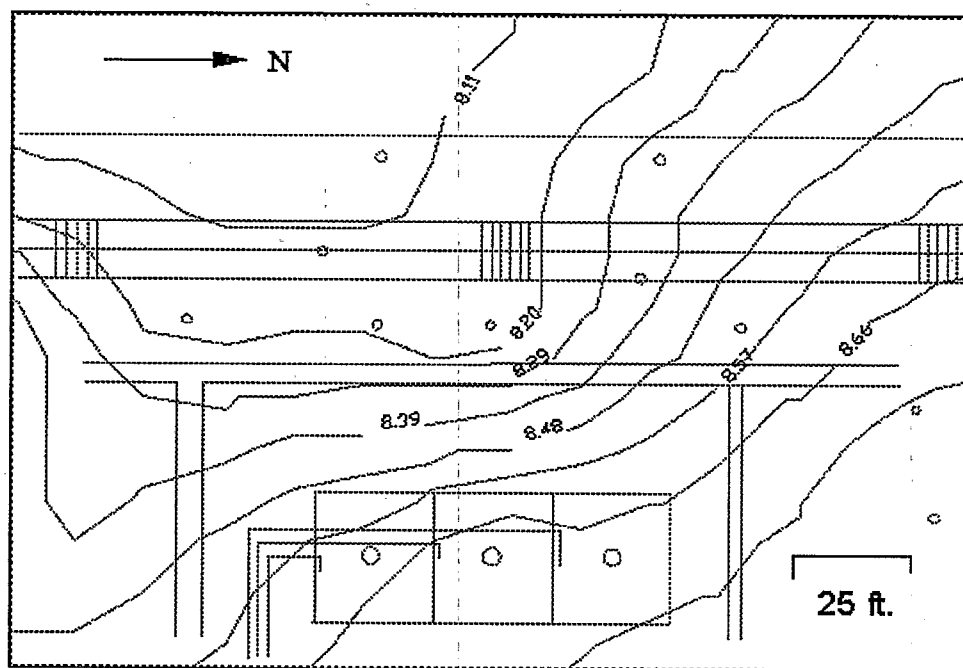
Figure 5-1. Plan map of xylene spill site.

Figure 5-2. Contour map of apparent free xylene thickness in feet.

Figure 5-3. Groundwater contours at spill site in feet.

The initial assessment activities focused on: (1) definition of project objectives, (2) development of a site conceptual model, and (3) selection of an appropriate model. In this study the objectives were to assess the contamination from the site characterization data and to evaluate remedial system designs to control the phase separated hydrocarbon source. Time was considered a major factor because it was recognized that a rapid remedial response would increase the volume of recoverable xylene and minimize the development residual NAPL. Specifically, it was speculated, based on normal weather patterns, that a significant rise in the water table would probably begin within approximately 4 months (120 days) of the release date. The site characterization investigation had taken 40 days, which left about 80 days to design, install, and implement the recovery system as well as recover the mobile xylene.

The site conceptual model derived from the characterization data consisted of a shallow, thin, unconfined aquifer that was underlain by an aquiclude. The unconfined portion of the aquifer was between 3.5 and 4 feet thick. This aquifer was relatively permeable and was considered isotropic and homogeneous. Dissolved, residual, and mobile free phase xylene was contained in the unsaturated and saturated portion of the aquifer.

73

An independent survey of available computer codes indicates that 6 models, ARMOS, MAGNAS, MOFAT, MOTRANS, SPILLCAD and SWANFLOW, could be utilized to model multiphase flow conditions at the site (*Weaver and Johnson*, 1993). However, due to limitations in site data and time constraints, it was considered necessary to utilize a practical, user-friendly code that could generate reasonably accurate results and would not require significant data input and setup time. Furthermore, the project objectives required the application of a multiphase flow model that could simulate remedial activities such that recoverable product volumes, residual product volumes, and the time of recovery could be estimated. Based on these needs, SPILLCAD (ES&T, 1994), a screening level model for evaluating the feasibility and effectiveness of recovery designs, was selected. SPILLCAD is an areal two-dimensional model that calculates mobile hydrocarbon volume, contaminated soil volume, recoverable hydrocarbon volume and residual hydrocarbon volume, and enables the flow field and time of recovery to be estimated using particle-tracking (pathline) analysis. Soil and fluid property values utilized in the modeling effort are presented in Table 5-1.

Table 5-1. Soil and Fluid Property Values for Model Simulations

$\rho_{ro}=0.86$	$K_{sw}=23.1 \, \text{ft} \, d^{-1}$	$S_m=0.13$
$\eta_{ro}=0.81$	$\phi=0.30$	$S_{og}=0.03$
$\beta_{ao}=2.30$	$\alpha=4.50 \, \text{feet}$	$S_{or}=0.26$
$\beta_{aw}=2.00$	$n=2.70$	

5.3 Model Results

The initial phase of the modeling study involved data entry of water and hydrocarbon elevations as measured in the installed wells. Using this data the volume of free xylene was estimated to be 172 gallons. The NAPL lens was over a 1400 square feet in area with the thickest portion of the lens occurring about 5 feet downgradient of the platform. Of particular concern was the fact that a considerable portion of the lens occurred underneath the railroad lines, thus, potentially complicating recovery. Using the initial information generated by the model, the next phase of the modeling effort addressed two aspects: (1) the design of an optimal recovery system that would minimize smearing of xylene and that would incorporate the physical constraints of the site and (2) evaluate the impact of water table fluctuations on the effectiveness of the recovery operations.

Three recovery systems were investigated. The first scenario involved locating the recovery well placed upgradient of the rail lines in the thickest zone of free xylene, the second scenario involved locating the recovery well downgradient of the rail lines, and the third scenario

entailed both of these well locations. Using these well locations, a variety of pumping rates were evaluated for each of the wells. As shown in Table 12 capture was obtained when pumping rates were at least 0.5 gpm for Scenarios 1 and 3 and 1.0 gpm for Scenario 2. Pumping rates greater than 1.25 gpm resulted in excessive drawdown corresponding to water levels below the pump elevation. Model results indicate that scenarios with pumping rates between 0.5 and 1.25 gpm yielded similar recovery (Table 5-2).

**Table 5-2. Results of SPILLCAD Modeling Simulations**

Pump-ing Rate Per Well (gpm)	Single Downgradient Well				Single Upgradient Well				Both Wells			
	Recov-ery (gal)	Residual (gal)		Cap-ture	Recov-ery (gal)	Residual (gal)		Cap-ture	Recov-ery (gal)	Residual (gal)		Cap-ture
		Unsat-urated	Satu-rated			Unsat-urated	Satu-rated			Unsat-urated	Satu-rated	
0.1	--	-	--	N	-	-	-	N	-	-	-	N
0.5	75	21	73	Y	-	-	-	-N	77	36	58	Y
1.0	76	37	58	Y	77	41	54	Y	71	66	35	Y
1.25	74	44	53	Y	75	49	48	Y	69	77	26	Y
1.5	Aquifer pumped past screen bottom											

Given these results, and in particular, the potential of smearing the hydrocarbon vertically within the soil profile, concern was then focused on how water table fluctuations might impact the recovery operations. The model enables the user to simulate regional water table fluctuations to evaluate the impact on recoverable hydrocarbon volume. This feature was found to be extremely useful, as the only other approach to obtain this information would have required the construction of a complex transient finite difference or finite-element model, which not only would have consumed valuable resources but also valuable time. Water table fluctuations of 1.5 and 0.75 feet were simulated for both well configurations at their optimal water pumping rates (Table 5-3). The results indicated that the seasonal water table fluctuations would decrease recoverable xylene volumes by 30 and 60 percent. Given that only half of the xylene could be recovered under even optimal conditions, it was considered imperative to complete recovery operations prior to the seasonal rise in groundwater levels to reduce long term cost and minimize dissolved impacts to the groundwater.

Table 5-3. Results of SPILLCAD Regional Water Table Fluctuations Simulations

Well Location & Pumping Rate (gal)	Fluctuation (ft)	Product Recovery (gal)	Residual (gal)	
			Unsaturated	Saturated
Upgradient (1.0 gpm)	0	77	41	54
	0.75	55	62	54
	1.5	36	82	54
Downgradient (0.5 gpm)	0	78	21	73
	0.75	49	50	72
	1.5	30	71	70
Two Wells (1.0 gpm total)	0	77	36	58
	0.75	55	58	58
	1.5	36	78	58

The final aspect of the modeling effort involved determining the time required to reach asymptotic recovery. More specifically, could the optimal recovery of 80 gallons of xylene be achieved within the eighty day time interval remaining prior to the advent of the seasonal rising water table using the rates and well locations previously defined. To address this issue, backward particle-tracking analysis was conducted for each of the recovery wells. Using the NAPL travel time analysis, it was determined that optimal recovery could occur within 60 days at each individual well. The downgradient recovery well could recover the lens at a pumping rate of 0.5 gpm while the upgradient well would require a pumping rate of 1.0 gpm. As shown in Figure 5-2, the distribution and length of the pathlines indicate that most of the plume north, south and east of the well is recovered prior to 60 days. However, areas southwest of the well do not become captured until 60 days (Figure 5-4). A third scenario was executed to determine the time of recovery if both wells were operational. A recovery rate of 0.5 gpm was defined for each well. This simulation resulted in a similar recoverable volume, but the time of recovery was decreased by 15 days.
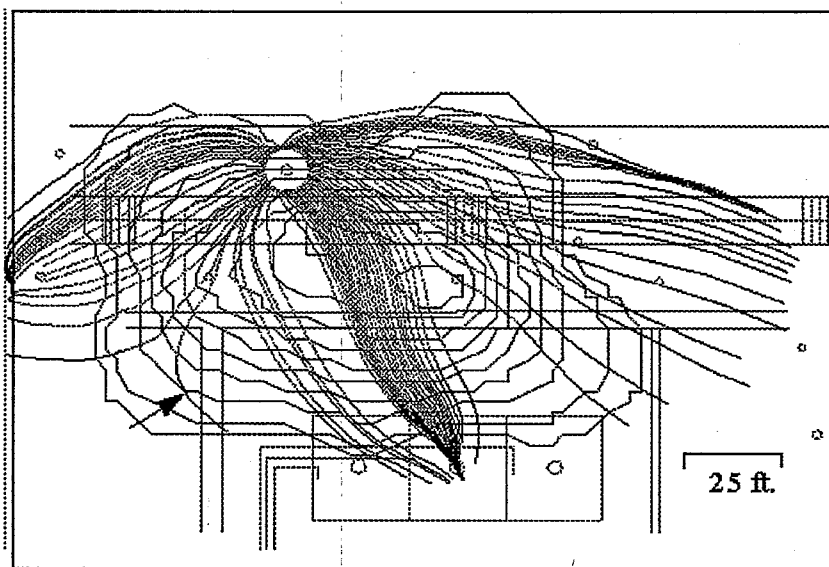
Figure 5-4. Results of particle-tracking analysis for two well scenario. Pathlines are based on a 60 day time of travel. Arrow indicates streamline that limits recovery time.

Information from the SPILLCAD modeling effort was used to determine the efficiency of the recovery system, as measured by volume of product recovered, relative to total fluids recovered. As shown in Table 5-4, the calculated efficiency ratios were determined to be 2.0, 1.1, and 0.9 gallons per 1000 gallons for the downgradient single well system, the two well system, and the upgradient single well system, respectively. Since the recoverable volume was similar for all three scenarios, the rate and recovery time were the primary variables affecting the efficiency. Hence, the most effective system was the downgradient single well as it produced the lowest volume of water. Hence, less water is pumped per volume of recovered xylene. The downgradient system was 1.8 times more efficient at product recovery than the two well system.

Table 5-4. Optimal Recovery Characteristics for Scenarios 1, 2, and 3

Well Location & Total Pumping Rate (gpm)	Recovery (gal)	Residual (gal)		Asymptotic Recovery Time	Water Pumped (X 1000 gal)	Oil - Water Cut (gal/1000 gal)
		Unsaturated	Saturated			
Upgradient Well (1 gpm)	77	41	54	60	86.4	0.9
Downgradient Well (0.5 gpm)	78	21	73	55	39.6	2.0
Both Wells (1.0 gpm)	77	36	58	45	64.8	1.1

5.4 Summary and Conclusions

The results of the SPILLCAD modeling effort provided critical information regarding possible remedial efforts at the release. This information included:

1)   Optimal xylene recovery was approximately 80 gallons,
2)   Optimal rates ranged from 0.5 to 1 gpm,
3)   Seasonal fluctuations decreased the volume of recoverable xylene by 30 and 60 percent,
4)   Optimal recovery could be achieved within 45 and 60 days, and
5)   The efficiency of the recovery systems ranged from 0.9 to 2.0 gallons recovered per 1000 gallons of water pumped.

Based on this modeling effort, the downgradient single well system appears to provide the needed results with the highest efficiency and the lowest capital costs. The other systems, although capable of producing a similar recovery volume, are not as efficient, and hence, will result in higher remedial costs.

Information from simple models can provide valuable information to evaluate remedial options. In this case study, the answers provided by modeling could not be obtained within the needed time frame by any other means. As a result, application of the models discussed in this report is proven to be an important tool for assessment of xylene contamination at the site as well as in the design of a recovery system. Although the constraints illustrated in this case study are possibly more severe than at most sites, the methods are broadly applicable and can be used at all sites to better assess, contain, and remediate hydrocarbon contaminants.

References

American Petroleum Institute. 1989. A Guide to the Assessment and Remediation of Underground Petroleum Releases, 2nd edition.

Arya, L. M. and J. F. Paris. 1981. A physicoempirical model to predict soil moisture characteristics from particle size distribution and bulk density data, Soil Sci. Soc. Am. J., 45, 1023-1030.

Baker, O. and W. Swerdloff. 1956. Finding surface tension of hydrocarbon liquids, oil and gas J., 125.

Carsel, R. F. and R. S. Parrish. 1988. Developing joint probability distributions of soil water retention characteristics, Water Resour. Res., 24, 755-769.

Conrad, S. H., J. L. Wilson, W. R. Mason and W. Peplinski. 1992. Visualization of residual organic liquid trapped in aquifers, Water Resource Res. 28: 467-478.

Dakin, R. A., Holmes, A. T. and Tiplady, D. J. 1992. Practical aspects of hydrogeology studies for hydrocarbon migration in British Columbia, Subsurface Contamination by Immiscible Fluids, K.U. Weyer (editor), A.A. Balkema, Rotterdam.

de Pastrovich, T. L., Y. Baradat, R. Barthel, A. Chiarelli and D. R. Fussell. 1979. Protection of groundwater from oil pollution, CONCAWE, Report 3/79, The Hague, 61 p.

Environmental Systems and Technologies, Inc. 1994c. SPILLCAD 3.2: Data Management and Decision Support for Hydrocarbon Spills, Blacksburg, VA.

Environmental Systems and Technologies, Inc. 1994b. SOILPROP: A Program to Estimate Unsaturated Soil Hydraulic Properties from Particle Size Distribution Data, Version 2.0, Blacksburg, VA.

Environmental Systems and Technologies, Inc. 1994a . ARMOS: Areal Multiphase Organic Simulator for Free Phase Hydrocarbon Migration and Recovery, Vers. 5.0, Blacksburg, VA.

Environmental Systems & Technologies, Inc. 1994. SPILLCAD 3.12: Data Management and Decision Support for Hydrocarbon Spills, Blacksburg, VA.

Farr, A. M., R. J. Houghtalen and D. B. McWorter. 1990. Volume estimation of light nonaqueous phase liquids in porous media, Ground Water, 28, 48-56.

Gruszcenski, T. S. 1987. Determination of a realsistic estimate of the actual formation product thickness using monitoring wells: a field bailout test, Proc. Petroleum Hydrocarbon in Groundwater: Prevention, Detection and Restoration, NWWA, Houston.

Hall, C. W. and J. A. Johnson. 1992. Limiting factors in groundwater remediation, Journal of Hazardous Materials, 32, 215-225, Elvesier Science Publishers, Amsterdam.

Hall, R. A., S. B. Blake and S. C. Champlin Jr. 1984. Determination of hydrocarbon thicknesses in sediments using borehole data, Proc. 4th Nat. Symp. on Aquifer Restoration and Ground Water Monitoring, NWWA, 300-304.

Hampton, D. R. and P. D. G. Miller. 1988. Laboratory investigation of the relationship between actual and apparent product thickness in sands, Proc. Petroleum Hydrocarbons and Organic Chemicals in Ground Water, NWWA.

Huntley, D. and R. N. Hawk. 1992. Non-aqueous phase hydrocarbon saturations and mobility in a fine-grained, poorly consolidated sandstone, Proc. Petrol. Hydrocarbons and Organic Chemicals in Groundwater, NGWA, Houston.

Kaluarachchi, J. J. and J. C. Parker. 1992. Multiphase flow in porous media with a simplified model for oil entrapment, Transport in Porous Media, 7, 1-14.

Kemblowski, M. W. and C. Y. Chiang. 1990. Hydrocarbon thickness fluctuations in monitoring wells, Ground Water, 28, 244-252.

Kool, J. B. and J. C. Parker. 1988. Analysis of the inverse problem for transient unsaturated flow, Water Resour. Res., 24, 817-830.

Lenhard, R. J. and J. C. Parker. 1987. Measurement and prediction of saturation-pressure relationships in three-phase porous media systems, J. Contam. Hydrol.,1, 407-424.

Land, C. S. 1968. Calculation of imbibition relative permeability for two- and three-phase flow from rock properties, Trans. Am. Inst. Min. Metall. Pet. Eng., 243, 149-156.

Lenhard, R. J., J. C. Parker and J. J. Kaluarachchi. 1988b. A model for hysteretic constitutive relations governing multiphase flow, 3. Refinements and numerical simulations, Water Resour. Res., 25, 1727-1736.

Lenhard, R. J. and J. C. Parker. 1990. Estimation of free hydrocarbon volume from fluid levels in observation wells, Ground Water, 28, 57-67.

Lyman, W. J., W. F. Reehl and D. H. Rosenblatt. 1982. Handbook of Chemical Property Estimation Methods, McGraw-Hill, New York.

Mishra, S., J. C. Parker and N. Singhal. 1989. Estimation of soil hydraulic properties and their uncertainty from particle size distribution data, J. Hydrol., 108, 1-18.

Ostendorf, D. W., R. J. Richards and F. P. Peck. 1993. LNAPL Retention in Sandy Soil, Ground Water, 31, 285-292.

Parker, J. C., R. J. Lenhard and T. Kuppusamy. 1987. A parametric model for constitutive properties governing multiphase flow in porous media, Water Resour. Res., 23, 618-624.

Parker, J. C., J. J. Kaluarachchi, V. J. Kremesec and E. L. Hockman. 1990. Modeling free product recovery at hydrocarbon spill sites, Proc. Petrol. Hydrocarbons and Organic Chemicals in Groundwater, NWWA.

Parker, J. C., J. J. Katyal, J. L. Zhu, V. J. Kremesec and E. L. Hockman. 1991. Free product recovery at spill sites with fluctuating water tables, Proc. 5th Nat. Outdoor Action Conf., NWWA.

Parker, J. C., J. Zhu and H. White. 1992. Modeling phase seperated hydrocarbon migration and recovery in anisotropic fractured media, Proc. Petroleum Hydrocarbons in Groundwater Conference, NGWA.

Parker, Jack C., A. K. Katyal, J. L. Zhu, V. J. Kremesec and E. L. Hockmann. 1994. Modeling free product migration and recovery at hydrocarbon spill sites, Ground Water, 32, 119-128.

van Dam, J. 1967. The migration of hydrocarbons in a water-bearing stratum, In: The Joint Problems of the Oil and Water Industries, P. Hepple, ed. Inst. Petrol., London, 55-96.

van Genuchten, M. Th. 1980. A closed-form equation for predicting the hydraulic conductivity of unsaturated soils, Soil Sci. Soc. Amer. J., 44, 892-898.

Weaver, J.W. and J.A. Johnson. 1993. Modeling for assessment of remediation of hydrocarbon spills, 3rd Annual Symposium on Groundwater and Soil Remediation, Quebec City, Quebec.

Wilson, J. L. 1992. Pore scale behavior of spreading and non-spreading organic liquids in the vadose zone, Subsurface Contamination By Immiscible Fluids. U. Weye,. Ed.:107-114, Rotterdam: Balkema.

Zhu, J. L., J. C. Parker, A. K. Katyal, V. J. Kremesec, E. L. Hockmann and M. N. Gallagher. 1991. Effects of delays in recovery system startup on product recovery at hydrocarbon spill sites, Proc. Conference on Hydrocarbons in Groundwater, NWWA.

81